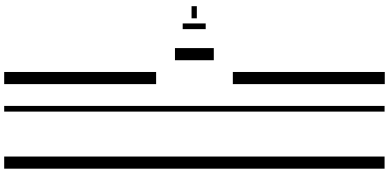

Minimal Surfaces in Riemannian Manifolds with Application to Shape Spaces

Masterarbeit
zur Erlangung des akademischen Grades
Master of Science

Westfälische Wilhelms-Universität Münster
Fachbereich Mathematik und Informatik
Institut für Numerische und Angewandte Mathematik

Betreuung:
Prof. Dr. Benedikt Wirth

Eingereicht von:
Christian Amrhein

Münster, Mai 2016

Zusammenfassung. Das Ziel dieser Masterarbeit ist die diskrete Version von Plateaus Problem in riemannschen Mannigfaltigkeiten zu lösen. Um die Existenz von kontinuierlichen Minimalflächen sicherzustellen, wurden zunächst die klassischen Resultate der Differentialgeometrie untersucht. Diese stellen jedoch zusätzliche Anforderungen an die riemannsche Mannigfaltigkeit, zum Beispiel nach oben beschränkte Schnittkrümmung und von der Null weg-beschränkten Injektivitätsradius. Daher wurden zusätzlich einige Resultate der Geometrischen Maßtheorie untersucht, die weniger Bedingungen an die Riemannschen Mannigfaltigkeiten stellen. Pinkall und Polthier entwickelten einen Algorithmus, um diskrete Minimialflächen im euklidschen Raum zu berechnen. Das Setting und der Algorithmus wurden, nach kleinen Anpassungen für Riemannsche Mannigfaltigkeiten, übernommen. Da es üblich ist, in Formen-Räumen (shape spaces) statt der echten Distanz eine (lokale) Approximation zu verwenden, wurde dem Algorithmus ein Verfeinerungsschritt für die Triangulierung hinzugefügt. Dieser stellt sicher, dass die Triangulierung die Mannigfaltigkeit fein genug auflöst, sodass die Distanz-Approximationen gut genug sind. Pinkall und Polthier zeigten, dass ihr Algorithmus im Dreidimensionalen konvergiert. Dies gilt allgemein für den endlich dimensionalen euklidischen Raum. Für allgemeine riemannsche Mannigfaltigkeiten existiert derzeit noch kein Beweis. Trotzdem wird der Algorithmus auf verschiedene Räume mit einer nicht-euklidischen Metrik angewandt: auf einen Raum mit einer deformierten euklidischen Metrik und auf zwei Formen-Räume, die der offen und geschlossen viskosen Stäben. Dabei zeigen die Experimente, dass der Algorithmus in einigen Fällen konvergiert, was aber stark abhängt von der Wahl der initialen Punkte und der Art der initialen Triangulierung.

Abstract. The aim of this master thesis is to solve the discrete version of Plateau's problem in Riemannian manifolds. For Riemannian manifolds with additional conditions with regard to the curvature and injectivity radius differential geometry provides the existence of (classical) minimal surfaces. Geometric measure theory can be used to show the existence for Riemannian manifolds with fewer constraints. Pinkall and Polthier developed an algorithm to compute discrete minimal surfaces in an Euclidean space. This setting and algorithm were used and adapted to work in Riemannian manifolds. In the setting of shape spaces distance approximations were used, which are only valid for points close to each other. This is why a refinement step was added to the algorithm, to show that a finer triangulation achieves no better optimum of the minimized Dirichlet energy. Pinkall and Polthier showed that their algorithm works in the three-dimensional Euclidean space. This theorem also valid for the finite-dimensional Euclidean space. The convergence of the algorithm for Riemannian manifolds is not yet shown. However, the algorithm was applied to a distorted Euclidean space and the shape spaces of open and closed viscous rods and several experiments show that the algorithm converges but depends on a good selection of initial points and the initial triangulation.

Eidesstattliche Erklärung

Hiermit versichere ich, *Christian Amrhein*, dass ich die vorliegende Arbeit selbstständig verfasst und keine anderen als die angegebenen Quellen und Hilfsmittel verwendet habe. Gedanklich, inhaltlich oder wörtlich übernommenes habe ich durch Angabe von Herkunft und Text oder Anmerkung belegt bzw. kenntlich gemacht. Dies gilt in gleicher Weise für Bilder, Tabellen, Zeichnungen und Skizzen, die nicht von mir selbst erstellt wurden.
Alle auf der CD beigefügten Programme sind von mir selbst programmiert worden.

Münster, 27.5.2016

Christian Amrhein

Contents

1 Introduction

Many famous mathematicians worked on the subject of minimal surfaces, one of the first who considered minimal surfaces was Joseph-Louis Lagrange in 1760. However, the problem of finding minimal surfaces for a given boundary curve is named after Joseph Plateau who worked with real world minimal surfaces, soap films spanned by a wire frame, in the 19th century. The first major breakthrough in finding a solution to the problem Lagrange stated was done by Jesse Douglas in 1931 [Dou31] and simultaneously by Tiber Radó in 1930 [Rad30]. In 1936 Douglas received one of the two first Fields Medals for his work on this problem. In the following decades mathematicians worked on extensions and modifications of this problem and a whole new area of mathematics was developed, the so-called geometric measure theory by Federer and Fleming in 1969 [Fed69].
The aim of this thesis is to study an algorithm to compute discrete minimal surfaces in Riemannian manifolds. The motivation for this is the application to shape spaces. Since minimal surfaces are the natural higher dimensional equivalent to geodesics and M. Rumpf and B. Wirth developed a variational approach to discrete geodesics [RW13] the question arised if this can be generalized to discrete minimal surfaces.
This thesis provides a proof-of-concept. It shows that there are solutions of Plateau's problem in general finite-dimensional shape spaces, that the proposed algorithm converges in finite-dimensional Euclidean space and that it converges in experiments for some shape spaces.
Such an algorithm may help to extend the theory of discrete differential geometry and has applications in computer science. For example, given several three-dimensional shapes which are modelled by vertices and edges as well as a meaning of a distance between such models a weighted interpolation of these shapes can be computed. This can improve existing shape classification based on discrete geodesic calculus.

This thesis is structured as follows. First, in chapter 2 the theory of discrete geodesics by M. Rumpf and B. Wirth is presented and gives a short introduction to continuous and discrete geodesics and shows an example.
Chapter 3 consists of three parts, section 3.1 explains the access to minimal surfaces through differential geometry. Since the results from differential geometry are not satisfactory, section 3.2 gives a short introduction to geometric measure theory and states the existence and regularity theorems that imply the existence of minimal surfaces in shape spaces that are explained in the section 3.3. The last section 3.4 gives a summary of the results which are the most relevant for the discrete setting and shape spaces.

In chapter 4 the discrete setting and the algorithm to compute discrete minimal surfaces are defined. The ideas and definitions originate in an algorithm from U. Pinkall and K. Polthier [PP93] for the three-dimensional Euclidean space. This algorithm was modified and extended to discrete surfaces in Riemannian manifolds. Furthermore, a convergence theorem of the original algorithm for finite-dimensional Euclidean space and some details on the implementation are given.
Here a convergence theorem for the finite-dimensional Euclidean space is given.
In the next chapter 5 experiments show how the algorithm performs in several different settings. Section 5.1 shows a classical setting in an Euclidean space with the standard metric where the convergence is expected and the following setting have increasing complexity of distance approximations, a distorted Euclidean metric, the shape space of open viscous rods and the shape spaces of closed viscous rods. In chapter 6 a summary of the results is drawn and an outlook is given that explains some promising ideas which could increase the performance of the algorithm and yield a convergence theorem for Riemannian manifolds.

2 Interpolation in Shape Spaces

In section 2.1 the preliminaries to Riemannian manifolds and continuous geodesics are defined, followed by the definition of the discrete counterparts of the geodesics and some properties of discrete geodesics in section 2.2. The third section 2.3 introduces the shape space of viscous rods and some computational experiments for this shape space are shown. In more detail shape spaces will be introduced in section 3.3.

2.1 Preliminaries

This section contains a list of definitions and properties for Riemannian manifolds. It defines the exponential map, injectivity radius, differential forms, outer derivative, Riemannian volume form.
In the following let $(\mathcal{M}, g)$ be an m-dimensional, *smooth, Riemannian manifold*, i.e. a smooth m-dimensional manifold $\mathcal{M}$ equipped with a Riemannian metric g. The Riemannian metric g is an inner product (i.e. a non degenerate, positive definite and symmetric bilinear form) which is defined on each tangent space $T_p\mathcal{M}$ and depends smoothly on the base point $p \in \mathcal{M}$.
Let $x = (x^1, \dots, x^m) : U \to \Omega \subset \mathbb{R}^m$ denote the local coordinates for an open subset $U \subset \mathcal{M}$. Then the Riemannian metric can be represented in these local coordinatesby a positive definite, symmetric matrix $(g_{ij}(x))_{i,j=1,\dots,m}$ where the coefficients depend smoothly on x.
A (smooth) *curve* Γ is a (smooth) map $[a, b] \to \mathcal{M}$ for $a < b \in \mathbb{R}$. It is called *closed* if $\Gamma(a) = \Gamma(b)$ and *simple* if the restriction $\Gamma|_{]a,b[}$ is injective. A closed, simple curve is also called *Jordan* curve.

The Riemannian metric is defined on the tangent space, however, it induces a metric on the manifold with the help of curves minimizing the length.

Definition 2.1 (Length and energy)**.** *Given a differentiable manifold $\mathcal{M}$ the length $L(\gamma)$ and energy $E(\gamma)$ of a smooth curve $\gamma : [a, b] \to \mathcal{M}$ where $a < b \in \mathbb{R}$ are defined as*

$$L(\gamma) := \int_a^b \|\dot{\gamma}(t)\| \, dt \tag{2.1}$$

and

$$E(\gamma) := \frac{1}{2} \int_a^b \|\dot{\gamma}(t)\|^2 \, dt, \tag{2.2}$$

where $\dot{\gamma}(t) = \frac{d\gamma}{dt}(t)$ *is the derivative of* $\gamma(t)$ *in the tangent space* $T_{\gamma(t)}\mathcal{M}$ *of* $\mathcal{M}$ *and* $\|\dot{\gamma}(t)\| = \sqrt{\langle \dot{\gamma}(t), \dot{\gamma}(t) \rangle}$ *with* $\langle\ ,\ \rangle$ *the scalar product in the tangent space.*

Theorem 2.2 shows that the energy is an upper bound for the length up to a constant factor.

Theorem 2.2. *Let* $\gamma : [a, b] \to \mathcal{M}$ *be a smooth curve then*

$$(L(\gamma))^2 \leq 2(b-a)E(\gamma) \tag{2.3}$$

and equality holds if and only if $\|\dot{\gamma}(t)\|$ *is constant.*
If γ *is parameterized proportionally to arc-length then*

$$L(\gamma) = 2 \cdot E(\gamma). \tag{2.4}$$

Proof. Consider the Hölder inequality

$$\int \|f(t)g(t)\|dt \leq \left(\int \|f(t)\|^2 dt \right)^{\frac{1}{2}} \left(\int \|g(t)\|^2 dt \right)^{\frac{1}{2}} \tag{2.5}$$

with $f(t) = \dot{\gamma}(t)$ and $g(t) = 1$. This yields

$$\begin{aligned}(L(\gamma))^2 &= \left(\int_a^b \|\dot{\gamma}(t)\|\, dt \right)^2 \leq \int_a^b \|\dot{\gamma}(t)\|^2 dt \cdot \int_a^b 1 dt = (b-a) \cdot \int_a^b \|\dot{\gamma}(t)\|^2 dt \\ &= 2(b-a)\frac{1}{2} \int_a^b \|\dot{\gamma}(t)\|^2 dt = 2(b-a) \cdot E(\gamma).\end{aligned}$$

Thus, equation (2.3) is proven.
The Inequality (2.5) is an equality if and only if $f(t) = c \cdot g(t)$. Here it means that $\|\dot{\gamma}(t)\| = c \cdot 1$ for a constant $c \in \mathbb{R}$.
Parameterized proportionally to arc-length means $a = 0$, $b = 1$ and $\|\dot{\gamma}\| = 1$, which implies the second statement (2.4). □

Theorem 2.3 (Distance)**.** *Let* $\mathcal{M}$ *be a Riemannian manifold,* p, $q \in \mathcal{M}$*. Then*

$$\begin{aligned}d(p,q) := \inf\{L(\gamma) \,|\gamma : [a,b] \to \mathcal{M} \text{ piecewise smooth curve} \\ \text{with } \gamma(a) = p,\ \gamma(b) = q\}\end{aligned}$$

defines a distance function and satisfies the usual axioms (positive definite, symmetric, triangle inequality).

The topology induced by this distance function d coincides with the original manifold topology on $\mathcal{M}$. A *geodesic* is the shortest curve between two (close) points and is typically defined as a solution to the Euler-Lagrange equation of the energy (2.2). Using the coordinates $(x^1(\gamma(t)), \ldots, x^m(\gamma(t)))$, the notation $\dot{x}^i(t) := \frac{d}{dt}x^i(\gamma(t))$, and

$$\Gamma^i_{jk} = \frac{1}{2} g^{il} \cdot (g_{jl,k} + g_{kl,j} - g_{jk,l}),$$

where

$$(g^{ij})_{i,j=1,\dots,m} = (g_{ij})^{-1} \text{ and } g_{jl,k} = \frac{\partial}{\partial x^k} g_{jl}$$

the Euler-Lagrange equations can be stated in local coordinates. The expressions Γ^i_{jk} are called Christoffel symbols.

Definition 2.4 (Geodesic)**.** *A smooth curve $\gamma : [a, b] \to \mathcal{M}$ for $a < b$ which satisfies*

$$\ddot{x}(t) + \Gamma^i_{jk}(x(t))\dot{x}^j(t)x^k(t) = 0 \text{ for } i = 1, \dots, m$$

is called a geodesic.

Due to Picard-Lindelöf's existence theorem for differential equations geodesics exist for a short time.

Theorem 2.5 ([Jos08, Theorem 1.4.2])**.** *Let $\mathcal{M}$ be a Riemannian manifold, $p \in \mathcal{M}$, $v \in T_p\mathcal{M}$. Then there exists $\varepsilon > 0$ and precisely one geodesic*

$$c : [0, \varepsilon] \to \mathcal{M}$$

with $c(0) = p$ and $\dot{c}(0) = v$. In addition, c depends smoothly on p and v.

This leads to the exponential map which diffeomorphically maps a neighbourhood of $0 \in T_p\mathcal{M}$ onto a neighbourhood of $p \in \mathcal{M}$.

Definition 2.6 (Exponential Map)**.** *Let $\mathcal{M}$ be a Riemannian manifold, $p \in \mathcal{M}$, then*

$$\begin{aligned} V_p :&= \{v \in T_p\mathcal{M} \mid c_v \text{ is defined on } [0, 1]\} \\ exp_p :&V_p \to \mathcal{M} \\ &v \mapsto c_v(1) \end{aligned}$$

is called exponential map.

Since for all $p \in \mathcal{M}$ there exists a small neighbourhood $U \subset \mathcal{M}$ such that exp_p maps U diffeomorphically onto a subset of $\mathbb{R}^m$, *normal*- and *polar*-coordinates can be defined that have an easy local representation of the metric g.

Definition 2.7 (Injectivity Radius)**.** *Let $\mathcal{M}$ be a Riemannian manifold, $p \in \mathcal{M}$. The injectivity radius of p is*

$$i(p) := \sup\{\rho > 0 \mid \exp_p \text{ is defined on } d_\rho(0) \subset T_p\mathcal{M} \text{ and injective}\}$$

where $d_\rho := \{y \in \mathbb{R}^m \mid \rho \geq \|y\|\} \subset T_p\mathcal{M}$. The injectivity radius of the manifold $\mathcal{M}$ is

$$i(\mathcal{M}) := \inf_{p \in \mathcal{M}} i(p).$$

Furthermore, locally a geodesic is a curve of minimal length [Jos08, Corollary 1.4.2].

Differential Forms The notations and definitions are taken from [Lan99]. One possibility how to introduce differential forms is to define what these locally on the tangent spaces and then glue this smoothly together.

Definition 2.8 (Differential Form, Wedge Product)**.** *Let V be an n-dimensional vector space. Then $Alt^k V$ marks the space of alternating k-forms, i.e. $\omega \in Alt^k V$ is a k-linear mapping $\Omega : \underbrace{V \times \cdots \times V}_{k} \to \mathbb{R}$ such that if $v_1, \ldots, v_k \in V$ are linearly dependent then $\omega(v_1, \ldots, v_k) = 0$.*
A differential k-form on a differentiable manifold $\mathcal{M}$ is defined as the mapping $\omega : \mathcal{M} \to Alt^k T_p\mathcal{M}$ which assigns each $p \in \mathcal{M}$ an alternating k-form $\omega_p \in Alt^k T_p\mathcal{M}$ and is differentiable in charts. The space of differential forms in denoted by $\Omega^k\mathcal{M}$. For $k = 0$, $\Omega^0\mathcal{M}$ is defined, due to consistency, as the space $C^\infty(\mathcal{M})$, the smooth functions from $\mathcal{M}$ to $\mathbb{R}$. These differential forms induce a so-called exterior algebra with the wedge product as the outer product. This is again defined locally. Let V be a vector space, $\omega \in Alt^r V$ and $\eta \in Alt^s V$. Then

$$\begin{aligned} \wedge : Alt^r V \times Alt^s V &\to Alt^{r+s} V \\ (\omega, \eta) &\mapsto \omega \wedge \eta \end{aligned} \tag{2.6}$$

is defined as the wedge product with

$$\omega \wedge \eta(v_1, \ldots, v_{r+s}) := \frac{1}{r!s!} \sum_{\tau \in S(r+s)} sgn(\tau) \cdot \omega(v_{\tau(1)}, \ldots, v_{\tau(r)}) \cdot \eta(v_{\tau(r+1)}, \ldots, v_{\tau(r+s)}).$$

Definition 2.9 (Outer Derivative d)**.** *There is a unique mapping $\Omega^k \xrightarrow{d} \Omega^{k+1}$ called outer derivative characterised by*

- *$df \in \Omega^1\mathcal{M}$ is the usual differential of f for $f \in \Omega^0\mathcal{M} = C^\infty(\mathcal{M})$;*
- *$d \circ d = 0$;*
- *$d(\omega \wedge \eta) = d\omega \wedge \eta + (-1)^r \omega \wedge \eta$ for $\omega \in \Omega^r$.*

The usual differential of $f \in C^\infty(\mathcal{M})$ in local coordinates x can be written as $(\frac{\partial f}{\partial x_i})_{i=1,\ldots,m}$.

A map $\phi : V \to W$ from one vector space to another induces a map from $Alt^k W$ to $Alt^k V$ by pulling back the values.

Definition 2.10 (Pullback)**.** *The pullback $\phi^* : Alt^k W \to Alt^k V$ for the vector spaces V and W of a map $\phi : V \to W$ is defined as*

$$(\phi^*\omega)(v_1, \ldots, v_k) = \omega(\phi(v_1), \ldots, \phi(v_k)) \tag{2.7}$$

for all alternating k-forms $\omega \in Alt^k W$. This structure extends to differentiable manifolds by applying this local definition the tangent spaces.

The top forms of an orientable differential manifold, i.e. forms in $\Omega^m\mathcal{M}$ where m is the dimension of $\mathcal{M}$, are special, since they can be integrated. There is one top form in Riemannian manifolds, the so-called Riemannian volume element, which gives a proper definition for the volume of a manifold.

Definition 2.11 (Riemannian Volume Element)**.** *Let $\mathcal{M}$ be an oriented Riemannian manifold, then*

$$\omega_{\mathcal{M}} := \sqrt{det(g_{ij})}dx^1 \wedge \cdots \wedge \cdot dx^m \tag{2.8}$$

is the Riemannian volume form in local coordinates $(x^1, \ldots, x^m)$.

2.2 Discrete Geodesic Calculus

In "Discrete Geodesic Calculus in Shape Space and Applications in the Space of Viscous Fluidic Objects." by M. Rumpf and B. Wirth [RW13] a discrete geodesic calculus was developed which allows to compute an approximation to a geodesic between two given objects in shape spaces. Shape spaces can be modelled by Riemannian manifolds. Section 2.3 will show an example of a shape space and section 3.3 gives a more detailed introduction to shape spaces. In the referenced paper the discrete counterparts of the continuous energy and length of curves are defined and it is shown that discrete curves converge to continuous geodesics for increasing number of points.
For a manifold $\mathcal{M}$ the discrete counterpart to a smooth curve γ is a discrete set of points, a so-called *discrete K-path* defined as a $(K+1)$-tuple $(y_0, \ldots, y_K)$ with $y_k \in \mathcal{M}$ for $k = 0, \ldots, K$. Since shape spaces are modelled by Riemannian manifolds, the exact distance between two shapes can be computed by the induced distance function. However, in most cases this is expensive, hence a distance approximation is used. Let $d(.,.)$ denote the exact distance induced by the Riemannian metric, then

$$W(x, y) \approx d^2(x, y) \tag{2.9}$$

gives a squared distance approximation which is valid for x close to y.

Definition 2.12 (Discrete Length and Energy)**.** *Let $y = (y_0, \ldots, y_K)$ be a discrete K-path, then the discrete length L and the discrete energy E are defined as*

$$L_{discrete}(y) = \sum_{k=1}^{K} \sqrt{W(y_{k-1}, y_k)} \tag{2.10}$$

and

$$E_{discrete}(y) = K \cdot \sum_{k=1}^{K} W(y_{k-1}, y_k), \tag{2.11}$$

where $W(.,.)$ is the squared distance approximation.

For the existence of an energy-minimizing K-path and the convergence of the discrete energy to the continuous energy see [RW13, Theorem 4.4, Corollary 4.10].

Length versus Energy

A intuitive idea to obtain a K-path of minimal length connecting two points p and q in $\mathcal{M}$ would be minimizing the length. However, there are several reasons why the energy is better suited. The two main reasons are

1. that minimizing the length does not necessarily converge to a length-minimizing curve for $K \to \infty$ due to the distance approximation

2. that the property of geodesics *parametrized by arc-length* translates to *equidistribution of the points* in the discrete setting. (Equidistribution is not guaranteed when minimizing the length, even in the continuous setting there exist curves of minimal length which are no geodesics).

The first reason can be explained by the following example. Consider figure 2.1 and assume that the surface $\mathcal{M}$ is embedded in $\mathbb{R}^3$ and $W(x, y) := \|x - y\|_3^2$, i.e. the Euclidean metric of $\mathbb{R}^3$, is used as distance approximation to the actual distance in $\mathcal{M}$ which is induced by shortest continuous curves in $\mathcal{M}$.

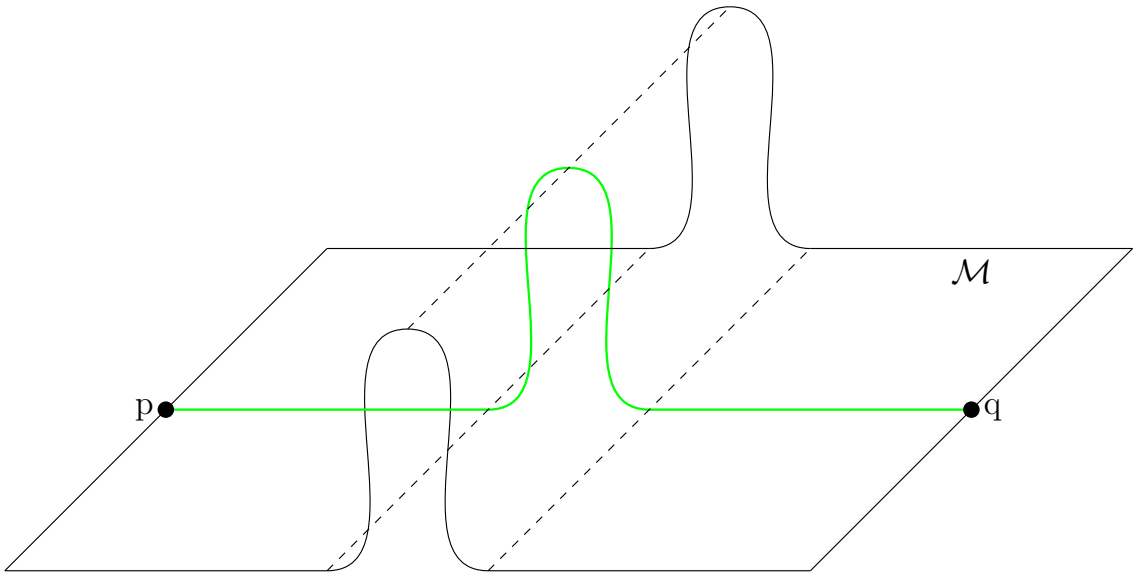

Figure 2.1: Assume that the surface $\mathcal{M}$ is embedded in $\mathbb{R}^3$. The curve connecting p and q represents a geodesic in the embedded manifold.

In this setting a valid K-path connection p and q is $\gamma = (\underbrace{p, \ldots, p}_{K\text{-times}}, q)$ with a discrete length $L(\gamma) = \|p - q\|_3$ which is lower than any continuous connecting curve in $\mathcal{M}$. The second reason consists actual of two statements, a theorem proves the equidistribution of points when minimizing the energy and an example shows that there are smooth curves of minimal length which are no geodesics.

Theorem 2.13. *Let $\gamma : [0,1] \to \mathcal{M}$ be a geodesic between p and q in $\mathcal{M}$ with $p \neq q$ close enough so that γ is unique. Let $y = (y_0, y_1, y_2)$ be a 2-path with $y_0 = p$ and $y_2 = q$. Then y minimizes the discrete energy if and only if $y_1 = \gamma(0.5)$ when using the exact distance as distance approximation.*

Remark: Here, as distance approximation the exact distance is used. [RW13] shows the equidistribution more generally, but theorem 2.13 is the core of the equidistribution.

Proof. The theorem is shown in two steps, first it is shown that y_1 has to be on the geodesic γ and second that $y_1 = \gamma(0.5)$. Both parts are proven by contradiction.
First assume that there is a $y_1 \neq \gamma(t)$ for all $t \in [0,1]$ such that $E_{discrete}(y)$ is minimal. Then with $l_1 := d(y_0, y_1)$ and $l_2 := d(y_1, y_2)$ the discrete energy of y can be computed as

$$E_{discrete}(y) = 2 \cdot (l_1^2 + l_2^2).$$

However, for $y_{opt} = \gamma(0.5)$ and $l_3 := d(y_0, y_{opt}) = d(y_{opt}, y_2)$ it holds that

$$l_1 + l_2 > d(y_0, y_2) = 2 \cdot l_3 \quad \Rightarrow \quad l_3 < \frac{l_1 + l_2}{2}.$$

since γ is the unique geodesic. Using $\tilde{y} = (y_0, \gamma(0.5), y_2)$ leads to

$$\begin{aligned} E_{discrete}(\tilde{y}) &= 4 \cdot l_3^2 < 2 \cdot \frac{(l_1 + l_2)^2}{2} \\ &= 2 \cdot \frac{1}{2}(l_1^2 + l_2^2) + 2 \cdot l_1 \cdot l_2 \leq \frac{1}{2} \cdot E_{discrete}(y) + \frac{1}{2} \cdot 2(l_1^2 + l_2^2) \\ &= E_{discrete}(y) \end{aligned}$$

which is a contradiction to the assumption. For the second part assume that there exists a $t_1 \in [0,1] \backslash \{0.5\}$ such that $E(y)$ is minimal. With the same notation as in the previous case, $l_3 = \frac{l_1 + l_2}{2}$ since geodesics are parametrized by arc length. However, since $l_1 \neq l_2$, it follows that

$$\begin{aligned} E_{discrete}(\tilde{y}) &= 4 \cdot l_3^2 = 2 \cdot \frac{(l_1 + l_2)^2}{2} \\ &= 2 \cdot \frac{1}{2}(l_1^2 + l_2^2) + 2 \cdot l_1 \cdot l_2 \underbrace{<}_{l_1 \neq l_2} \frac{1}{2} \cdot E_{discrete}(y) + \frac{1}{2} \cdot 2(l_1^2 + l_2^2) \\ &= E_{discrete}(y). \end{aligned}$$

□

An example of a length-minimal smooth curve which is no geodesic is the curve $\gamma : [0,1] \to \mathbb{R}^3$ with the standard metric which connects x and y by a line with a non-constant derivative

$$\gamma(t) = x + \sin(t \cdot \frac{\pi}{2}) \cdot (y - x).$$

The curve has $L(\gamma) = \|x - y\|_3$, the same length as a geodesic. The energy, however, is a lot worse $E(\gamma) = \frac{\pi}{4}\|x - y\|_3^2$.

2.3 Interpolation of Viscous Rods

A simple shape space is the space of viscous rods, which was also used in [RW15]. For now it suffices to know about shape spaces that they are a set of two- or three-dimensional objects which are homotopy equivalent to one or multiple reference objects with a Riemannian metric, which induces a distance function. In most cases the computation of the exact distance is expensive. That is why distance approximations are used. A more detailed introduction to shape spaces will be done in chapter 3.3.
The discretisation of this shape space simplifies a viscous rod to a polygonal line of straight rods glued together. The space of such rods can be classified into so-called closed and open viscous rods. For a closed rod the start point and end point have to coincide, for an open rod there is no additional constraint. The distance defined on this shape space describes the physical effort it takes to stretch or bend one rod into another. The approximation to the squared distance in terms of lengths and angles of the rod is as follows. Given two rods γ, β with $\gamma = (l_1^\gamma, \dots, l_n^\gamma, \alpha_1^\gamma, \dots, \alpha_n^\gamma)$ and $\beta = (l_1^\beta, \dots, l_n^\beta, \alpha_1^\beta, \dots, \alpha_n^\beta)$ then

$$W(\gamma, \beta) = \sum_{i=1}^{n} \frac{(l_i^\gamma - l_i^\beta)^2}{l_i^\gamma} + 2 \cdot \sum_{i=1}^{n} \frac{(\alpha_i^\gamma - \alpha_i^\beta)^2}{l_i^\gamma + l_{i+1}^\gamma}. \tag{2.12}$$

Here l_i^γ and α_j^γ describe the lengths of the straight segments and the angles at the vertices, respectively. The first term of (2.12) considers the stretching and the second term the bending. These can be weighted separately by adding constant factors to the functional. Figure 2.2 shows an example of a discrete, closed rod.

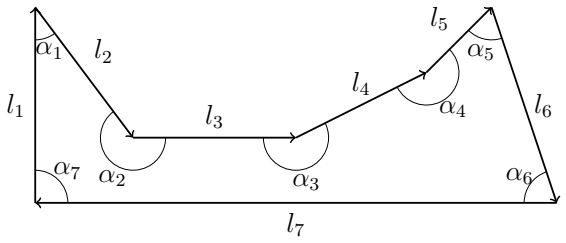

Figure 2.2: Example of a closed rod where the lengths and angles are indicated.

Typically elements in shape spaces are equivalence classes, where the relation is induced by translation and rotation invariance and sometimes scale invariance. This makes Euclidean interpolation impossible, unless a standard representative is fixed. Nevertheless, figure 2.3 shows a K-path, obtained by choosing the same representative (obtained by setting the first point to $(0, 0)$ and fixing the the direction of the first segment) and taking an Euclidean average of the coordinates of the vertices.
The discrete energy of this curve is $L_{discrete}(\gamma) = 3.639$ computed with the shape space distance approximation of equation 2.12. The next figure 2.4 shows a discrete geodesic. This example clearly shows that even for a few points, the differ-

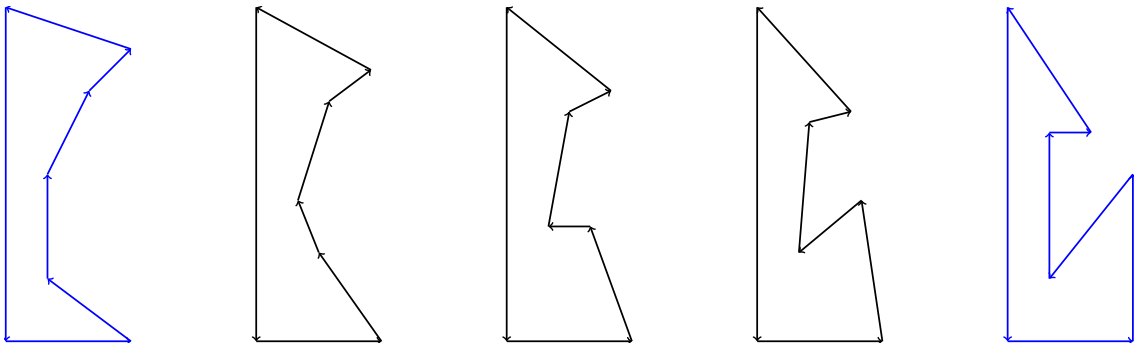

Figure 2.3: Discrete curve which minimizes the Euclidean distance. The blue shapes mark the two initial given objects of the shape space. The discrete K-path is drawn in black. $L_{discrete}(\gamma) \approx 3.639$

ences between the two interpolations are obvious. This discrete geodesic is computed as minimizer of the discrete energy introduced earlier, the discrete length is $L_{discrete}(\gamma) = 2.208$.

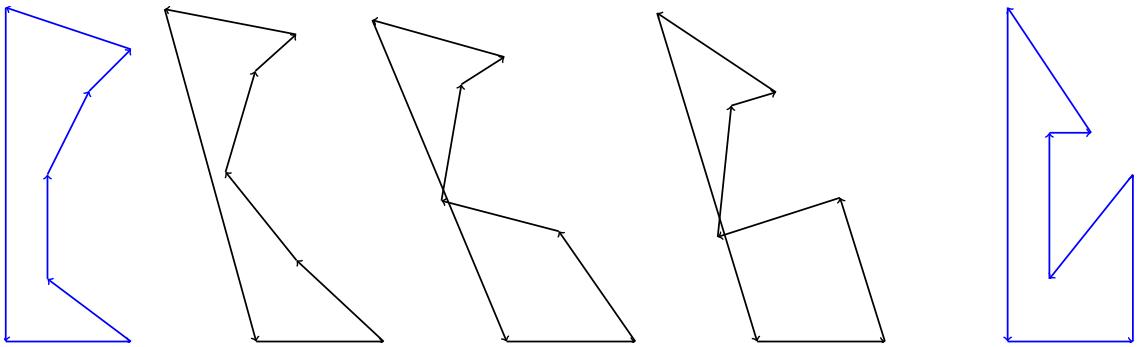

Figure 2.4: Discrete curve which minimizes the shape space distance approximation of the closed viscous rods. The blue shapes mark the two initial given objects of the shape space. The discrete K-path is drawn in black. $L_{discrete}(\gamma) \approx 2.208$

3 Theoretical Setting and Existence

Searching for minimal surfaces with a given boundary is called "Plateau's Problem". It consists in finding a surface of least area which is bounded by a given curve. Section 3.1 considers Plateau's Problem for Riemannian manifolds in terms of area and Dirichlet energy. It shows why the energy functional is better suited to solve Plateau's Problem than the area. This is followed by an overview of some classical results, beginning with Douglas and Radó who were the first who showed the existence of a solution in some generality. This section closes with a modern existence theorem from differential geometry, theorem 3.13.
The second section 3.2 deals with so-called integral currents, the generalisation of smooth surfaces in the setting of geometric measure theory. This approach was chosen since there are more general existence and regularity results for higher dimensions and codimensions. And last, in section 3.3, shape spaces are explained in more detail with some references.

3.1 Plateau's Problem for Riemannian Manifolds

This section states Plateau's problem for Riemannian manifolds which were introduced in the previous chapter 2.1. The aim of this chapter is to give an overview of the classical results from differential geometry and an existence theorem for harmonic maps which implies a solution to Plateau's problem. First the definitions of area and Dirichlet energy for manifolds are given and compared. To understand the following section, basic knowledge about differential geometry is needed. The main reference for this introduction is [Jos08]. Dierkes et. al. cover the three-dimensional case of the problem of Plateau in detail in [DJK$^+$10b], [DJK$^+$10c] and [DJK$^+$10a].With the application to shape spaces in mind some simplifications were made.

3.1.1 Area Minimization

Originally the idea was to find a surface of least area, which is bounded by a wire frame (or multiple wires).
The surface is usually a *Riemannian surface*, that is a one-dimensional complex manifold [Jos08, Definition 8.2.1]. However, most of the following definitions and theorems regarding minimal surfaces are restrained to the unit disk in $\mathbb{R}^2 = \mathbb{C}$

$$D = \{z \in \mathbb{C} \mid z = u + iv,\ \|z\| < 1\} \tag{3.1}$$

which has as boundary $\partial D = S^1$ the standard 1-sphere, which suffices for the application of disk-type minimal surfaces.

There exists a definition for an area or more general a volume of a manifold with the help of the Riemannian volume element.

Definition 3.1 (Area)**.** *The area of an orientable smooth Riemannian manifold $(\mathcal{M}, g)$ is defined as*

$$A(\mathcal{M}) = \int_{\mathcal{M}} \omega_{\mathcal{M}} \tag{3.2}$$

if the integral exists, where $\omega_{\mathcal{M}} = \sqrt{\det g_{ij}}\, dx^1 \wedge \cdots \wedge dx^n$ is the Riemannian volume element.

The higher-dimensional equivalent is sometimes denoted by $A^m(\Omega)$ for $\Omega \subset \mathbb{R}^m$ to mark the dimension of the surrounding space. One flaw of the here used Lebesque-measure is that if Ω is a subset of $\mathbb{R}^m$ with $A^m(\Omega) < \infty$ then $A^{m+1}(\Omega) = 0$ for the natural embedding of Ω in $\mathbb{R}^{m+1}$.

Definition 3.2 (Area)**.** *The area of a smooth map $f : D \to \mathcal{M}$ is defined as*

$$A(f) = \int_D f^* \omega_{\mathcal{M}} \tag{3.3}$$

where $f^*\omega_{\mathcal{M}}$ is the pull back of the differential form $\omega_{\mathcal{M}}$.

This area can be computed by

$$\begin{aligned} A(f) &= \int_D \sqrt{det(J(f)^t \cdot J(f))} du dv \\ &= \int_D \|f_u \wedge f_v\| \end{aligned}$$

where $J(f)$ is the Jacobi matrix of f and the area is invariant under reparametrisations. This leads to the classical problem of Plateau.

Definition 3.3 (Plateau's Problem, Area)**.** *Let Γ be a simple, closed curve in $\mathcal{M}$, then $f : \bar{D} \to \mathcal{M}$ is a solution to Plateau's problem if it fulfills the following conditions:*

1. *$f \in C^0(\bar{D}, \mathcal{M}) \cap C^2(D, \mathcal{M})$;*
2. *$A(f)$ is minimal;*
3. *The restriction $f_{\partial D}$ of f to the boundary ∂D of the parameter domain D is a homeomorphism of ∂D onto $im(\Gamma)$.*

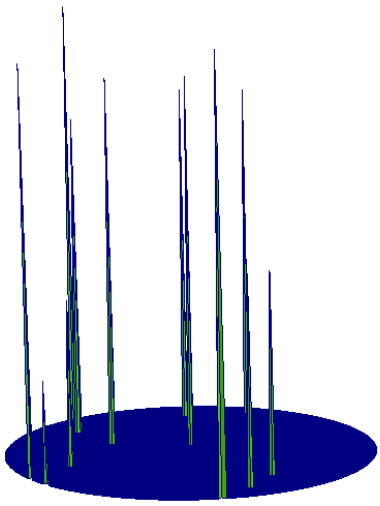

Figure 3.1: Plane unit disk with hairs.

Similar to the minimization of the energy and length of curves, the class of surfaces of least area for a given boundary contain undesired surfaces. Figure 3.1 gives an example of an unwanted surfaces. Since hairs, as straight lines, have zero area such hairs do not increase the total area. Such a surface with hairs can be represented by a smooth map [DJK+10b, p. 50]. However, as theorem 3.6 will show, a conformal map which minimizes the Dirichlet energy also minimizes the area. Hence, it was proposed by Hilbert to minimize the Dirichlet energy instead [DJK+10b, p. 248].

3.1.2 Dirichlet Energy Minimization

Definition 3.4 (Dirichlet energy)**.** *Let $f : D \to \mathcal{M}$ be a smooth map the Dirichlet energy is defined as*

$$E_D(f) = \frac{1}{2}\int_D tr(J(f)^t \cdot J(f))du \cdot dv = \frac{1}{2}\int_D (\|f_u\|^2 + \|f_v\|^2)du \cdot dv. \tag{3.4}$$

Functions which are critical points of equation 3.4 are called harmonic, this property is sometimes denoted by $\Delta f = 0$ which refers to the Laplace-Beltrami Operator Δ. [Jos08, Lemma 8.1.1].

Definition 3.5 (Conformal)**.** *A C^1-map $f : D \to N$ is called conformal if*

$$\|f_u\|^2 = \|f_v\|^2 \text{ and } \langle f_u, f_v\rangle = 0. \tag{3.5}$$

Theorem 3.6. *Let $(\mathcal{M}, g)$ be a finite dimensional Riemannian manifold. Let $D \subset \mathbb{R}^2$ be the standard disk bounded by the unit circle and $f : D \to \mathcal{M}$ a differentiable map, then*

$$E_D(f) \leq A(f) \tag{3.6}$$

and equality holds if and only if the map f is conformal.

Proof. By comparing the integrands of energy and area

$$E_D(f) = \frac{1}{2}\int_D (\|f_u\|^2 + \|f_v\|^2) du dv$$
$$A(f) = \int_D \|f_u \wedge f_v\| du dv$$

the desired result can be shown. The wedge product satisfies the Lagrange-identity

$$\begin{aligned} \|f_u \wedge f_v\| &= \sqrt{\|f_u\|^2\|f_v\|^2 - \|\langle f_u, f_v\rangle\|^2} \\ &\leq \|f_u\| \cdot \|f_v\| \qquad (3.7) \\ &\leq \frac{1}{2}(\|f_u\|^2 + \|f_v\|^2) \qquad (3.8) \end{aligned}$$

and so the inequality is shown. For equality in the case of conformal mappings the inequalities 3.7 and 3.8 need to be sharpened. These two inequalities are equations if and only if f is conformal. □

Now the definition of Plateau's problem 3.3 can be reformulated with the help of the Dirichlet energy and a solution of the Dirichlet version of Plateau's problem implies a solution of the Area version.

Definition 3.7 (Plateau's Problem, Dirichlet)**.** *Given a simple closed curve Γ in $\mathcal{M}$, then $f : \bar{D} \to \mathcal{M}$ is a solution to Plateau's problem for the boundary contour if it fulfills the following conditions:*

1. *$f \in C^0(\bar{D}, \mathcal{M}) \cap C^2(D, \mathcal{M})$;*
2. *The surface f satisfies in D the conditions:*
   a) *f is a critical point of the Dirichlet energy functional.*
   b) *$\|f_u\|^2 = \|f_v\|^2$, $\langle f_u, f_v\rangle = 0$, i.e. f is conformal.*
3. *The restriction $f_{\partial D}$ of f to the boundary ∂D of the parameter domain D is a homeomorphism of ∂D onto $im(\Gamma)$.*

3.1.3 Classical Existence Theorems

Plateau's problem was first formulated in 1760 by Lagrange, but it was first solved to some generality in 1930 simultaneously by Radó and Douglas.

Theorem 3.8 (Radó 1930)**.** *For any Jordan curve Γ in $\mathbb{R}^3$ which bounds at least one continuous surface with a finite area both versions of Plateau's Problem have a common solution.*

Radò showed that there are infinitely many solutions to the problem of least area and with the additional constraint to the boundary curve he showed that there is a solution to Plateau's problem, which implies that there is a minimal surface as a solution to the problem of least area.

Theorem 3.9 (Douglas 1931)**.** *For any Jordan curve Γ in $\mathbb{R}^n$, $n \geq 2$ there is a solution to the problem of Plateau.*

With another approach J. Douglas could solve Plateau's problem for a general n-dimensional Euclidean space and by a limit-process he got rid of the additional constraint that there must exist a continuous surface of finite area bounded by the boundary curve. For this work, Douglas was awarded with one of the first two Fields medals in 1936.
In 1937 Courant extended Plateau's problem to multiple Jordan curves ([Cou37]). More relevant to the setting of this thesis is the work of C. B. Morrey in 1948 [Mor48]

Theorem 3.10 (Morrey 1948)**.** *Let $(\mathcal{M}, g)$ be a homogeneously regular, finite-dimensional Riemannian manifold, and Γ a Jordan curve in $\mathcal{M}$, then there exists a solution to Plateau's problem.*
If $\mathcal{M}$ is smooth, then the minimal surface is at least two-times differentiable on the interior.

Homogeneously regular was introduced by Morrey in [Mor48, p. 838] and is a condition to the metric in local coordinates.

Definition 3.11 (Homogeneously regular)**.** *A differentiable Riemannian manifold $\mathcal{M}$ is said to be homogeneously regular if there exist numbers k and l (independent of x_0) with $0 < k \leq l$, such that any point x_0 in $\mathcal{M}$ lies in an open set in $\mathcal{M}$ which can be mapped on the unit hypercube $R : |x^i| < 1$ by a differentiable map such that x_0 corresponds to the origin and the $g_{\alpha\beta}(x)$ satisfy the condition that*

$$k \sum_{i=1}^{m} (\xi^i)^2 \leq \sum_{\alpha,\beta} g_{\alpha\beta}(x) \xi^\alpha \xi^\beta \leq l \sum_{i=1}^{m} (\xi^i)^2 \tag{3.9}$$

for all $(x^1, \ldots, x^m)$ on $\mathbb{R}$ and all $(\xi^1, \ldots, \xi^m)$.

Every compact manifold is homogeneously regular. For (non-compact) complete manifolds this is equivalent to bounded from below injectivity radius and bounded sectional curvature. There exists even more theory for minimal hypersurfaces and surfaces of higher codimensions (see for example [HKW76]) but restrictive requirements to the underlying Riemannian manifold are needed as well.

3.1.4 Existence of Conformal and Harmonic Mappings

In this thesis a more modern existence theorem based on differential geometry by J. Jost is presented. As in most approaches to Plateau's problem only the existence of a harmonic map is considered. This is based on the fact that there always exists a reparametrisation to a conformal mapping under which the Dirichlet energy is unchanged. This is the so-called Lichtenstein's theorem.

For a smooth map $f : D \to \mathcal{M}$ the Dirichlet energy is invariant under composition with a conformal diffeomorphism $\tau : D \to D$

$$E_D(f) = E_D(f \circ \tau). \tag{3.10}$$

This can be shown using the complex structure of the surface and the transformation rule for integrals. More details can be found in [HW07] or [Cou50].

If a Dirichlet minimizer is found, Lichtenstein's theorem provides the existence of a conformal reparametrisation.

Theorem 3.12 (Lichtenstein's theorem)**.** *Let $\Omega \subset \mathbb{R}^2$ be a subset bounded by a closed Jordan curve Γ of class $C^{m,\alpha}$ for a given $m \in \mathbb{N}$ and $\alpha \in (0,1)$, and let $(g_{jk}(x))$ be a positive definite, symmetric 2-matrix-valued function on $\bar{\Omega}$ with $g_{jk} \in C^{m-1,\alpha}(\bar{\Omega})$. Then there exists a conformal mapping τ from $\bar{D}$ onto $\bar{\Omega}$ which is of class $C^{m,\alpha}(\bar{D}, \mathbb{R}^2)$.*

To apply this theorem to a harmonic map $f : D \to \mathcal{M}$, take Ω as D with the metric g_{ik} induced by the pullback of the Riemannian metric from $\mathcal{M}$ via f. Then there is a map $\tau : \bar{D} \to \bar{D}$ which is conformal with respect to the induced and Euclidean metric. Then $f \circ \tau : D \to \mathcal{M}$ is conformal and harmonic.

As a consequence of theorem 3.6 conformal and harmonic maps are local area minimizers, and because of the reparametrisation of Lichtenstein the existence of harmonic maps implies the existence of area minimizers. In differential geometry there are several theorems covering existence of harmonic mappings (see [Jos08] and [HW07]). One existence result without overly restrictive requirements is the following.

Theorem 3.13 ([Jos08, Theorem 8.3.2])**.** *Let $\mathcal{M}$ be a complete Riemannian manifold with sectional curvature K bounded from above by κ and injectivity radius i_0 greater than 0, and $p \in \mathcal{M}$. Let*

$$0 < r < \min\left(\frac{i_0}{2}, \frac{\pi}{2\sqrt{\kappa}}\right). \tag{3.11}$$

Let $\Gamma : \partial D \to B_r(p)$ be continuous and admitting an extension $\bar{f} : D \to B_r(p)$ of finite energy where $B_r(p) := \{q \in \mathcal{M} \mid d(q,p) \leq r\}$ is a geodesic ball in $\mathcal{M}$ with radius r.
Then there exits a harmonic map

$$f : D \to B_r(p) \subset \mathcal{M} \tag{3.12}$$

with

$$f|_{\partial D} = \Gamma \tag{3.13}$$

and f minimizes the Dirichlet energy among all such maps.
The modulus of continuity of f is controlled by r, κ, $E_D(\bar{f})$ and the modulus of Γ,

i.e. given $\varepsilon > 0$, there exists $\delta = \delta(r, \kappa, \Gamma) > 0$ such that $|x_1 - x_2| < \delta$ implies $d(f(x_1), f(x_2)) < \varepsilon$. Finally, for any $\sigma > 0$ the modulus of continuity of f on $\{z : |z| \leq 1 - \sigma\}$ is controlled by σ, r, κ and $E_D(\bar{f})$.

For the theorem, complete is to be understood with respect to the distance. Furthermore, the sectional curvature of a manifold is needed which is usually defined via the Riemannian curvature tensor [Jos08, Definition 3.3.2]. This definition and the proof of theorem 3.13 are omitted since a lot of additional results from differential geometry are needed.

3.2 Geometric Measure Theory

Another approach to finding minimal surfaces is through geometric measure theory. It is based on the work of Federer [Fed69] and can be seen as differential geometry, generalised through measure theory. First steps towards a better understanding of this theory were done by Morgan [Mor88] and De Lellis [DLS11].
Two main aspects of geometric measure theory are abstracting surfaces to currents and using the Hausdorff measure (or in general not the Lebesgue measure). Currents were developed by De Rham in 1955 and extended in "Normal and Integral Currents" by Federer and Fleming [FF60] in 1960.

Theorem 3.13 developed in the previous section about harmonic maps from differential geometry needs the curvature to be bounded from above and the injectivity radius to be bounded from below. These are rather strong requirements, since the sectional curvature of shape spaces is often unknown. There are several other results emerging from differential geometry [HW07], always having additional requirements to the manifold like non-positive curvature. The result geometric measure theory aims for is more general and the goal for this thesis is the following conclusion.

Theorem 3.14 ([XDC88])**.** *Any null homologous curve on a Riemannian manifold bounds a least area surface, which is a classical minimal surface in the interior.*

Here, null homologous means that the curve is contractible to a point. All of the following definitions and results are done for closed subsets of $\mathbb{R}^n$, since each m-dimensional Riemannian manifold can be smoothly embedded as a closed subset in $\mathbb{R}^n$ for $n \geq 2m + 1$. It can even be approximated by an isometric embedding.

Theorem 3.15 (Withney embedding theorem)**.** *A smooth m-dimensional manifold can be smoothly embedded in $\mathbb{R}^{2m+1}$ as a closed subset.*

Theorem 3.16 (Nash isometric embedding theorem)**.** *Let $(\mathcal{M}, g)$ be an m-dimensional Riemannian manifold and $f : \mathcal{M} \to \mathbb{R}^n$ a smooth embedding with $n \geq m + 1$. Then for arbitrary $\varepsilon > 0$ there exists an embedding $f_\varepsilon : \mathcal{M} \to \mathbb{R}^n$ which is*

1. *in class C^1,*

2. *isometric,*

3. *ε-close to f, i.e.:* $||f(x) - f_\varepsilon(x)|| < \varepsilon \; \forall x \in \mathcal{M}$.

Therefore, it suffices to find a minimal surface for a closed subset K of $\mathbb{R}^n$. Usually, the dimensions are denoted by $m+n$ for the manifold where m is the dimension of the current, the so-called codimension. If the manifold is embedded, n marks the dimension of the surrounding Euclidean space and the dimension of the manifold is denoted by $m + \bar{n}$.

In the next section 3.2.1 the currents and Hausdorff measure are introduced and it is shown that *area-minimizing* currents minimize the typical area (if this term is applicable). Section 3.2.2 states the existence and regularity results, this is done without proof, but further references are will be given.

3.2.1 Federer-Fleming Theory of Integral Currents

The following definitions are taken from C. De Lellis [DL11] and L. Simon [Sim83] with references to the original work of H. Federer [FF60], F. J. Almgren [Alm93], and S. Xu-Dong Chang [XDC88] unless stated otherwise.
This chapter introduces the generalisation of surfaces and shows that the mass of a current coincides with the area of the corresponding surface if one exists.
Let $\Omega_c^m(\mathbb{R}^{n+m}) \subset \Omega^m(\mathbb{R}^{n+m})$ denote the space of smooth, compactly supported m-forms (denoted by $D^m(\mathbb{R}^{n+m})$ in [Fed69, Section 4.1.7]) as a subspace of the smooth m-forms.
The *support* $spt(\omega)$ of a smooth m-form is the closure of the subset $U \subset \mathbb{R}^{n+m}$ s.th.

$$\forall x \in U\colon \omega(x) \neq 0. \tag{3.14}$$

The so-called *currents* are elements of the dual space and are denoted by $D_m\mathbb{R}^{n+m}$. Note that the $\mathbb{R}^{n+m}$ in $\Omega^m(\mathbb{R}^{n+m})$ and $D_m(\mathbb{R}^{n+m})$ is dropped if the context is clear.

Definition 3.17 (Current, De Rham, [DL11])**.** *An m-dimensional current T is a continuous linear map $T : \Omega_c^m(\mathbb{R}^{n+m}) \to \mathbb{R}$. The term continuity is to be interpreted in the following sense. $T(\omega_k) \to T(\omega)$ whenever $\omega_k \subset \Omega_c^m$ is a sequence such that*

1. *there exists an open subset $\Omega \subset \mathbb{R}^{m+n}$ with $\bar{\Omega} \subset \mathbb{R}^{m+n}$ compact such that $spt(\omega_k) \subset \Omega$ for all k. (This property is sometimes denoted by $\Omega \subset\subset \mathbb{R}^{m+n}$);*

2. *the sequence $\omega_k \to \omega$ converges in $C^j(\Omega)$ for all j.*

This can be made local by taking a subset $U \subset \mathbb{R}^{n+m}$ and defining the currents as the dual space of $\Omega_c^m(U)$. The support $spt(T)$ of a current T is the complement of the maximal open set U for which $T(\omega) = 0$ whenever $spt(\omega) \subset U$ (see [Fed69, Section 4.1.1]).

With the standard definition of $\mathcal{D}^0 = C_0^\infty(\mathbb{R}^{n+m})$ as the smooth functions with compact support, the zero-dimensional currents are the distributions. Using the standard topology on $D_m(\mathbb{R}^{n+m})$ (see [Sim83]) a sequence of m-dimensional currents T^k converges to T if $T^k(\omega) \to T(\omega)$ for every $\omega \in \Omega_c^m(\mathbb{R}^{n+m})$. Using the differential for smooth forms the boundary of a current can be consistently defined.

Definition 3.18. *(Boundary, De Rham) An $(m-1)$-dimensional current S is the boundary of an m-dimensional current T if*

$$T(d\omega) = S(\omega) \quad \textit{for every } \omega \in \Omega_c^m. \tag{3.15}$$

S will then be denoted by ∂T.

Application to Surfaces

Each smooth m-dimensional oriented surface Σ in $\mathbb{R}^{n+m}$ induces a current $[\![\Sigma]\!]$ by integration

$$\begin{aligned} [\![\Sigma]\!] : \Omega_c^m(\mathbb{R}^{m+n}) &\to \mathbb{R} \\ \omega &\mapsto \int_\Sigma \omega \end{aligned} \tag{3.16}$$

over m-forms. The boundary of a current is consistent with the boundary of a surface by Stokes theorem.

$$\int_\Sigma d\omega = \int_{\partial\Sigma} \omega$$

Hausdorff Measure, Mass and Comass

Definition 3.19 (Hausdorff Measure)**.** *The Hausdorff measure $\mathbb{H}^m(A)$ for a subset $A \subset \mathbb{R}^n$ and a nonnegative integer m is defined as*

$$\mathbb{H}^m(A) := \lim_{\delta \to 0} \inf_{\substack{A \subset \cup S_j \\ diam(S_j) \le \delta}} \sum \alpha_m \left(\frac{diam(S_j)}{2} \right)^m \tag{3.17}$$

where the diameter of S is

$$diam(S) = \sup\{\|x - y\| \ \mid x, y \in S\} \tag{3.18}$$

and α_m is the m-dimensional Lebesgue volume of the m-dimensional unit ball $B_1^m(0)$.

This definition can be extended to any nonnegative real number m by setting

$$\alpha(m) = \Gamma\left(\frac{1}{2}\right)^m / \Gamma\left(\frac{m}{2} + 1\right) \tag{3.19}$$

with $\Gamma(n)$ the usual Gamma function. Observe that $\mathbb{H}^0$ equals the counting measure and if $\mathbb{H}^m(A) < \infty$ then $\mathbb{H}^k(A) = 0$ for any $m < k < \infty$.

Recall that a simple m-vector is an element of $\Lambda_m(\mathbb{R}^{m+n})$ of the form $v_1 \wedge \cdots \wedge v_m$ and there is a natural length of a simple m-vector, $|v_1 \wedge \cdots \wedge v_m|$, the m-dimensional Hausdorff measure of the parallelogram spanned by the vectors $v_1, \ldots, v_m$.[1]
Ω_c^m induces a norm on D_m, the dual norm. Another dual pair are the so-called *mass* and *comass*.

Definition 3.20 (Comass)**.** *Let $\omega \in \Omega_c^m$. Then the comass of ω is the norm*

$$\|\omega\|_c := \max\{\langle \omega(p), v_1 \wedge \cdots \wedge v_m \rangle \mid p \in \mathbb{R}^{n+m},\ |v_1 \wedge \cdots \wedge v_m| = 1\} \tag{3.20}$$

where $\langle \cdot, \cdot \rangle$ is the inner product on Ω^m naturally induced.

Simon shows, how an inner product is naturally induced in his lecture notes [Sim83]. He also defines the norm and dual norm on currents without the comass and uses $|\omega| = \sup_{p \in U} \langle \omega(x), \omega(x) \rangle^{\frac{1}{2}}$. This leads to the same mass.

Definition 3.21 (Mass)**.** *Let $T \in D_m \mathbb{R}^{n+m}$. The mass of T is defined as*

$$M(T) := \sup_{\|\omega\|_c \leq 1} T(\omega), \tag{3.21}$$

or localised

$$\|T\|(\Omega) = \sup_{\substack{\omega \in \Omega_c^m \\ spt(\omega) \in \Omega \\ \|\omega\|_c \leq 1}} T(\omega). \tag{3.22}$$

One important theorem of geometric measure theory is that the mass of a current induced by a surface coincides with the area of the surface. This is based on the so-called area formula and leads to area-minimizing currents.

Theorem 3.22 (Area Formula)**.** *Suppose $f : \mathbb{R}^m \to \mathbb{R}^n$ is smooth and injective with $m \leq n$ and $U \subset \mathbb{R}^m$ is Lebesgue $\mathbb{L}^m$-measurable then*

$$\int_U f^* \omega_{\mathbb{R}^n} = \mathbb{H}^m(f(U)) \tag{3.23}$$

where $\omega_{\mathbb{R}^n}$ is the Riemannian volume element of $\mathbb{R}^n$.

Remark Federer and Simon proved this theorem for Lipschitzian not necessarily injective functions. Equation 3.23 is then

$$\int_U J_m f(x) d\mathbb{L}^m x = \int_{\mathbb{R}^n} N(f|U, y) d\mathbb{H}^m y.$$

Here $J_m f(x) = \sqrt{|J^t f(x) \cdot Jf(x)|}$ for $Jf(x)$ the Jacobian of f. Thus, the left hand side coincides with $\int_U f^* \omega_{\mathbb{R}^n}$. On the right hand side $N(f|U, y)$ is the multiplicity

[1] In the previous section this was defined with the help of the Lebesgue measure, but as a following theorem states, in this case they coincide.

and can be defined by $N(f|U,y) := \mathbb{H}^0(f^{-1}(\{y\})) \cap U$. Since in theorem 3.22 f is required to be injective, $N(f|U,y) = 1_{f(U)}$ and thus

$$\int_{\mathbb{R}^n} N(f|U,y) d\mathbb{H}^m y = \int_{\mathbb{R}^n} 1_{f(U)} d\mathbb{H}^m y = \mathbb{H}^m(f(U))$$

Last it remains to show that $M(\llbracket\Sigma\rrbracket) = \mathbb{H}^m(\Sigma)$ for an m-dimensional surface Σ. Therefore,

$$A^m(\Sigma) = \sup_{\substack{\omega \in \Omega_c^m \\ \|\omega\|_c \leq 1}} \int_\Sigma \omega.$$

Thus,

$$M(\llbracket\Sigma\rrbracket) = A^m(\Sigma).$$

Simon shows this in detail in his lecture notes [Sim83, p. 133].

Existence of Mass Minimizers and Integral Currents

Functional analysis shows that there exist mass minimizing currents [DL11].

Theorem 3.23 (Existence, De Lellis)**.** *Let Z be an $(m-1)$-dimensional current and $\bar{T}$ an m-dimensional current with $\partial\bar{T} = Z$ and $M(\bar{T}) < \infty$. Then there is a current T_0 such that $\partial T_0 = Z$ and*

$$M(T_0) = \min\{M(T) \mid \partial T = Z\}. \tag{3.24}$$

If $spt(\bar{T}) \subset K$ for some closed set K there exists a current T_0 such that $\partial T_0 = Z$, $spt(T_0) \subset K$ and

$$M(T_0) = \min\{M(T) \mid \partial T = Z \text{ and } spt(T) \subset K\}. \tag{3.25}$$

However, this yields unsatisfactory currents, see for example the Lavrentiv gap in [DL11]. This is why the class of currents is restricted to integral currents, defined in [Fed69, 4.1.24] or simplified in [DL11].

Definition 3.24 (Integer Rectifiable and Integral Currents)**.** *A current T is integer rectifiable if there are a sequence of oriented C^1 surfaces $\Sigma_i \subset \mathbb{R}^{m+n}$, a sequence of pairwise disjoint closed subsets $K_i \subset \Sigma_i$ and a sequence of positive integers k_i such that*

$$\sum_i k_i A^m(K_i) < \infty \tag{3.26}$$

$$T(\omega) = \sum_i k_i \int_{K_i} \omega \qquad \forall \omega \in \mathcal{D}^m \tag{3.27}$$

T is integral if both T and ∂T are integer rectifiable.

The mass of an integral current is then $M(T) = \sum_i k_i A^m(\Sigma_i)$. Surfaces are obviously integral and searching in this class of minimizers avoids the Lavrentiv gap, but to assert that the current of the minimizing process is again integral is no easy task.
This definition of integer rectifiable currents can be made local, by saying the conditions of 3.24 are satisfied for the restriction $T \llcorner \Omega$ to any bounded open set $\Omega \subset \mathbb{R}^{n+m}$.

3.2.2 Compactness and Existence

The space of integer rectifiable currents is not a vector space any more, so there is no simple functional-analytic principle which provides a good compactness property. However, this is needed for extracting a convergent subsequence. A fundamental result in the theory of Federer and Fleming is that the space of integral currents is compact in a suitable sense.

Theorem 3.25 (Compactness of integral currents)**.** *If T^k is a sequence of integral m-dimensional currents such that*

$$sup_k(M(T^k) + M(\partial T^k)) < \infty \tag{3.28}$$

then there is a subsequence, not relabelled, and an integral m-dimensional current T such that $T^k \to T$.

The compactness theorem 3.25 provides the existence of mass minimizing integer rectifiable currents in analogy to theorem 3.23.

Corollary 3.26 (Existence)**.** *Let Z be an $(m-1)$-dimensional integer rectifiable current and $\bar{T}$ an m-dimensional integral current with $\partial \bar{T} = Z$ and $M(\bar{T}) < \infty$. Then there is an integer rectifiable current T_0 such that $\partial T_0 = Z$ and*

$$M(T_0) = \min\{M(T) \mid T \text{ is integer rectifiable, } \partial T = Z\}. \tag{3.29}$$

If $spt(\bar{T}) \subset K$ for some closed set K then there exists an integer rectifiable current T_0 such that $\partial T_0 = Z$, $spt(T_0) \subset K$ and

$$M(T_0) = \min\{M(T) \mid T \text{ is integer rectifiable, } \partial T = Z \text{ and } spt(T) \subset K\}. \tag{3.30}$$

One interesting result is a theorem which shows that finite mass implies that the boundary is integer rectifiable.

Theorem 3.27 (Boundary rectifiability)**.** *If T is integer rectifiable and $M(\partial T) < \infty$ then T is integral.*

Furthermore, for a boundary current there is an extension with bounded mass.

Theorem 3.28 (Isoperimetric inequality)**.** *There is a $C > 0$ depending on the dimensions m and n with the following property. Let S be an integer rectifiable m-dimensional current in $\mathbb{R}^{m+n}$ with $\partial S = 0$. Then there is an integral current T with $\partial T = S$ and*

$$M(T) \leq C(M(S))^{(m+1)/m}. \tag{3.31}$$

Area Minimizing Currents and Regularity of Area Minimizing Currents

The following regularity theorems are not only valid for solutions of corollary 3.26, but for a class of integer rectifiable currents which are so-called area-minimizing which is a more general concept. This overview is based on [DL11]. Each solution of 3.26 is, in fact, area-minimizing.

Definition 3.29 (Area-Minimizing)**.** *Let $\Omega \subset \mathbb{R}^n$ be open and $\Sigma \subset \mathbb{R}^n$ be a smooth complete submanifold without boundary of dimension $m + \bar{n}$. An m-dimensional integer rectifiable current T is area-minimizing in $\Sigma \cap \Omega$ if*

- *$spt(T) \subset \Sigma$;*
- *$M(T + \partial S) \geq M(T)$ for every $(m+1)$-dimensional integral current S with $spt(S) \subset \Sigma \cap \Omega$.*

The first item ensures that T lies in Σ and the second item shows that no variation of T has lower mass, which corresponds to minimal area. The analysis of the regularity consists in defining the set of non regular points.

Definition 3.30. *$p \in spt(T) \backslash spt(\partial T)$ is an interior regular point if there is a positive radius $r > 0$, a smooth embedded submanifold Γ of Σ and a positive integer Q such that $T \llcorner B_r(p) = Q[\![\Gamma]\!]$. The set of interior regular points, which of course is relatively open in $spt(T) \backslash spt(\partial T)$, is denoted by $Reg(T)$. Its complement $spt(T) \backslash (spt(\partial T) \cup Reg(T))$, the interior singular set of T, is denoted by $Sing(T)$.*

The previous theorem 3.26 stated the existence of area-minimizing currents. The following theorems summarise the existing regularity theorems for the codimension 1 case and higher codimensions.

Theorem 3.31 (Regularity in codimension 1)**.** *Let $\Omega \subset \mathbb{R}^n$ be open, $\Sigma \subset \mathbb{R}^n$ be a smooth complete submanifold without boundary of dimension $m + 1$ and T an m-dimensional area-minimizing current. Then the following holds.*

1. *For $m \leq 6$, $Sing(T) \cap \Omega$ is empty (Fleming and De Giorgi ($m = 2$)), Almgren ($m = 3$), Simons ($4 \leq m \leq 6$).*
2. *For $m = 7$, $Sing(T) \cap \Omega$ consists of isolated points (Federer).*
3. *For $m \geq 8$, $Sing(T) \cap \Omega$ has Hausdorff dimension at most $m - 7$ (Federer) and it is countably $(m-7)$-rectifiable, namely, up to a set of $\mathbb{H}^{m-7}$-measure zero, it can be covered by countably many C^1 surfaces of dimension $m - 7$ (Simon).*
4. *The results (2)-(3) are optimal, namely for every $m \geq 7$ there are area-minimizing integral currents T in the Euclidean space $\mathbb{R}^{m+1}$ for which $Sing(T)$ has positive $\mathbb{H}^{m-7}$ measure (Bombieri-De Giorgi-Giusti).*

Theorem 3.32 (Regularity in codimension $\bar{n} \geq 2$)**.** *Let $\Omega \subset \mathbb{R}^n$ be open, $\Sigma \subset \mathbb{R}^n$ be a smooth complete submanifold without boundary of dimension $m + \bar{n}$ and T an m-dimensional area-minimizing current. Then for $\bar{n} \geq 2$ the following holds.*

1. *For $m = 1$, $Sing(T) \cap \Omega$ is empty.*
2. *For $m \geq 2$, $Sing(T) \cap \Omega$ has Hausdorff dimension at most $m - 2$ (Almgren).*
3. *Result (2) is optimal, namely for every $m \geq 2$ there are area-minimizing integral currents T in the Euclidean space $\mathbb{R}^{m+2}$ for which $Sing(T)$ has positive $\mathbb{H}^{m-2}$ measure (Bombieri-De Giorgi-Giusti).*

The second result was sharpened by Chang for two-dimensional area-minimizing currents.

Theorem 3.33 ($m = 2, \bar{n} \geq 2$)**.** *Assume that Ω, Σ are as in definition 3.29 and T an area-minimizing current, $\bar{n} \geq 2$ and $m = 2$. Then $Sing(T) \cap \Omega$ consists of isolated points.*

With this theorem Chang concludes the statement in theorem 3.14.

3.3 Shape Spaces

Shape spaces model two- or three-dimensional geometric objects and are often used in statistics and computer vision. They were introduced in 1977 by D. G. Kendall. At first, an object in a shape space was modelled as a finite set of vertices with a centre point modulo the rotation group. In this thesis I follow the general approach [KBCL09, Chapter 11] also followed by M. Rumpf and B. Wirth in [RW13]. Here, an object in a shape space is modelled as a closed subset of $\mathbb{R}^2$ or $\mathbb{R}^3$. The space is equipped with a Riemannian metric. Therefore, it can be seen as an infinite Riemannian manifold. Discretizing these closed subsets leads to finite-dimensional Riemannian manifolds.

A shape space is always based on a fixed reference model which is a closed subset $v \subset \mathbb{R}^d$ and as such describes the shape of the shape space $\mathcal{O}$. Then the underlying set for $\mathcal{O}$ is induced by all closed subsets u which are homotopy equivalent to v. To enforce a more differentiable structure, the homotopy equivalence is sometimes replaced by homeomorphisms or diffeomorphisms. In most cases, the interesting part are the deformations of the objects in shape spaces and not the location or orientation, so-called rigid body transformations. Translation and rotation induce an equivalence class $\sim$ on the closed sets in $\mathbb{R}^n$.

Definition 3.34 (Infinite-Dimensional Shape Space)**.** *For a closed subset $v \subset \mathbb{R}^d$ the shape space induced by v is defined as*

$$\mathcal{O} := \{u \subset \mathbb{R}^d \mid u \text{ closed, } u \text{ and } v \text{ are homotopy equivalent}\}/\sim \tag{3.32}$$

where the equivalence relation $\sim$ is induced by translation and rotation.

A geometrical interpretation of the tangent space of $\mathcal{O}$ at u are deformations of u, i.e. the velocity fields $u \to \mathbb{R}^d$.
Adding a Riemannian metric on the tangent space leads to infinite-dimensional Riemannian manifolds.

Example 3.35. *Take the unit circle S^1 in $\mathbb{R}^2$ as reference object v. Let*

$$\mathcal{M} := \mathcal{E}(S^1, \mathbb{R}^2)/\sim \cup \sim'$$

be the space of all smooth embeddings up to reparametrisations, rotations and translations, i.e. $\sim$ is induced by translation and rotation and $\sim'$ is induced by diffeomorphisms $\tau : S^1 \to S^1$. The additional equivalence relation $\sim'$ is needed to ignore parametrisations of S^1. This set is isomorphic to a subset of $\mathcal{O}$ induced by v since in $\mathcal{O}$ only homotopy equivalence was requested and for $f, g \in \mathcal{E}(S^1, \mathbb{R}^2)$, $f(S^1)$ is diffeomorphic to $g(S^1)$. The tangent space to $f \in \mathcal{E}(S^1, \mathbb{R}^2)$ is a subset of the space of smooth functions from S^1 to $\mathbb{R}^2$. These functions are velocity fields to S^1 and describe deformations of $f(S^1)$. A Riemannian metric is then a map

$$g_f : T_p\mathcal{M} \times T_p\mathcal{M} \to \mathbb{R}$$

which is symmetric, positiv definit and linear and smooth in $p \in \mathcal{M}$.

Fletcher and Whitaker considered the space of solid shapes in [FW06] in detail. The shape space $\mathcal{O}$ can be simplified to finite-dimensional manifolds by using a discrete set of points for the shapes with a connectivity specified by a so-called *simplical complex*.
A *k-simplex* for $k > 3$ is the higher-dimensional equivalent of points, edges and triangles, so-called zero-, one- and two-simplices, and the faces of a triangle are all edges and vertices of that triangle, the faces of an edge are the two vertices of that edge. A set of simplices creates a (simplicial) *k-complex* $\mathcal{K}$ if

- for each m-simplex in $\mathcal{K}$, $m \leq k$;
- the faces of each simplex are in $\mathcal{K}$;
- the intersection of two simplices in $\mathcal{K}$ is $\emptyset$ or a face of both.

An *abstract* simplicial complex, or the type of a simplicial complex refers to the adjacency of the vertices and not the location of the vertices. So, two simplicial complexes of the same type have a one-to-one correspondence of points, edges and triangles. The exact location of these points can, however, differ from one to the other.

Definition 3.36 (Shape Space)**.** *For a fixed finite simplicial complex v in $\mathbb{R}^d$, $d = 2$ or 3, the shape space induced by v is defined as*

$$\begin{aligned}\mathcal{O} := \{u \mid\ & u \text{ is a simplicial complex of the same type as } v \\ & \text{and } u \text{ is homotopy equivalent to } v\}/\sim.\end{aligned} \tag{3.33}$$

With an equivalence relation $\sim$ induced by translation and rotation invariance.

Since all objects $v \in \mathcal{O}$ can be described by a tuple of k points in $\mathbb{R}^d$ and a fixed abstract simplicial complex, $\mathcal{O}$ can locally be seen as $\mathbb{R}^{k \cdot d}$. Again with a Riemannian metric on the tangent space, this leads to finite-dimensional Riemannian manifolds.

Example 3.37. *Take S^1 the unit circle in $\mathbb{R}^2$ as reference object v, discretized by k-points. The corresponding shape space is then the shape of closed viscous rods, as in 2.3. Kendall systematically explores such spaces in [Ken89] where his pre-shape spaces are the equivalent to the shape spaces introduced here. His shape spaces ignore also scaling of the objects.*

3.4 Summary

With the help of geometric measure theory it can be concluded that for a shape space modelled by a smooth finite-dimensional Riemannian manifold and a Jordan curve as boundary which admits an extension to a disk-type surface of finite area there exists a solution of Plateau's problem. The interesting fact of this theory is that it shows also the limits of such a general approach. The two-dimensional case of minimial surfaces is a special case where only zero-dimensional sets violate the smoothness of the resulting surface. And even further regularity results state that these sets of singular points in two dimensions consist only of isolated points. In higher-codimensions the singular sets occur and are higher dimensional.
This general result helps when the injectivity radius and curvature are unknown or too expensive to compute to show that minimal surfaces exist. However, in most cases the application in mind is of local character. That means that the given Jordan curve may lie in a geodesic ball $B_\rho(p)$ around a point p, for such a setting the differential geometry results suffice. Furthermore, the differential geometry approach is better understood and may be better suited to help establish a convergence theorem for algorithms computing discrete minimial surfaces.

4 Discretisation and Algorithms

Most algorithms solve Plateau's problem by applying a two-step algorithm. They alternate between seeking a harmonic mapping and a conformal reparametrisation. One flaw of such algorithms is that each step could violate the previous result. The main idea for the algorithm implemented in this master thesis originates from the paper "Computing Discrete Minimal Surfaces and their Conjugate" by U. Pinkall and K. Polthier ([PP93]). They proposed a one-step algorithm to minimize the Dirichlet energy of maps $f : \Omega \to \mathbb{R}^3$, where $\Omega \subset \mathbb{R}^2$, with a fixed boundary curve Γ, such that $f(\partial\Omega) = \Gamma$. The trick of Pinkall and Polthier's algorithm is that they do not try to minimize the typical Dirichlet energy $E_D(f) = \frac{1}{2}\int_\Omega \|\nabla f\|^2$ but instead they stepwise minimize the Dirichlet energy of the flow $\min_f \frac{1}{2}\int_{\Sigma_i} \|\nabla f : \Sigma_i \to \mathcal{M}\|^2$ from a given surface Σ_i to the next surface in the manifold $\mathcal{M}$.
This chapter first defines the discrete setting in section 4.1 and next the algorithm in section 4.2 where it is proven that the algorithm converges for the finite-dimensional Euclidean space in theorem 4.7. Then details on the implementation are given in section 4.3.

4.1 Discrete Setting

The previous chapter 3 introduced the continuous setting for Plateau's problem. In this section, the results are transferred to a discrete setting. The following definitions, lemmas and propositions are taken from [PP93], with some small modifications.

The discrete counterpart of a continuous surface is based on triangles. More technically this can be seen again as a simplicial two-complex which was introduced in section 3.3.
An additional property for discrete surfaces needed is that they must be homogeneous which means that each one-simplex is the face of a two-simplex, and each zero-simplex the face of a one-simplex. Therefore, it suffices to note all triangles for a homogeneous simplicial two-complex.

Definition 4.1 (Discrete Surface)**.** *A discrete surface Σ in $\mathbb{R}^n$ is a connected homogeneous simplicial two-complex*

$$\Sigma := \{\Delta_0, \ldots, \Delta_N\} \tag{4.1}$$

consisting of a finite number of triangles Δ_i for $0 \leq i \leq N$. The triangles may be degenerated. A connected homogeneous simplicial two-complex is also called triangulation.

In this setting a triangle is degenerated if one angle of the triangle is 0 or π, whis implies that all angles of that triangle are degenerated. The area of a discrete surface is defined as the summation over the areas of the triangles.

$$A(\Sigma) := \sum_{i=0}^{N} A(\Delta_i) \tag{4.2}$$

Definition 4.2 (Area-Minimal)**.** *A discrete surface is (locally) area-minimal if and only if small perturbations of surface vertices in a small region increase the total area.*

Let

$$f : \Sigma_1 \to \Sigma_2 \tag{4.3}$$

be a map between two triangulations with the same underlying topology, i.e. the abstract simplicial complexes of Σ_1 and Σ_2 are identical which means that they have corresponding triangles, edges and vertices. Assume that f is defined on the vertices and continued as a linear map into the interior of the triangles. With this the energy of a map between discrete surfaces can be defined for a general energy functional E.

Definition 4.3 (Energy)**.** *The energy of a map between discrete surfaces is the sum over the energies of all linear triangular mappings*

$$f_i : \Delta_{1,i} \to \Delta_{2,i} \tag{4.4}$$

where $\Delta_{1,i}$ and $\Delta_{2,i}$ are the i-th corresponding triangles from Σ_1 to Σ_2 mapped onto each other by f_i.

$$E(f) = \sum_{i=1}^{n} E(f_i) \tag{4.5}$$

Definition 4.4 (Energy-Minimal)**.** *A discrete surface is (locally) energy-minimal if and only if small perturbations of surface vertices in a small region increase the total energy.*

Pinkall and Polthier found in [PP93] an easy way to compute the Dirichlet energy where the dependencies on the domain and image triangulation are clear.

Theorem 4.5. *Let $f : \Delta_1 \to \Delta_2$ be a linear map between the two triangles Δ_1 and Δ_2. Then*

$$E_D(f) = \frac{1}{4} \sum_{i=1}^{3} \cot \alpha_i \cdot a_i^2. \tag{4.6}$$

where α_i and a_i are opposite angle and length as in figure 4.1.

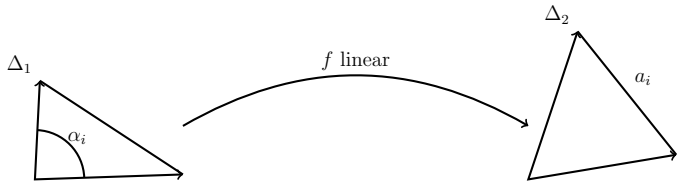

Figure 4.1: Linear mapping $f : \Delta_1 \to \Delta_1$.

Proof. The Dirichlet energy is computed as in the continuous setting (definition 3.4) on each triangle as

$$E_D(f) = \frac{1}{2}\int_{\Delta_1} |\nabla f|^2 = \frac{1}{2}\int_{\Delta_1} tr\ J(f)^t \cdot J(f).$$

To compute the integral first a two-dimensional representation for $tr\ (J(f)^t \cdot J(f))$ needs to be found and then the integral can be solved.
Since f is a linear mapping from one triangle-simplex to another and has a two-dimensional tangent space, f can be seen as a linear mapping from $\mathbb{R}^2 \to \mathbb{R}^2$. Assume Δ_2 is the simplex specified by three points $h_0, h_1, h_2 \in \mathbb{R}^n$, Δ_1 by $g_0, g_1, g_2 \in \mathbb{R}^n$ and Δ_e the standard simplex in $\mathbb{R}^2$ specified by $e_0 = (0 \quad 0)^t$, $e_1 = (1 \quad 0)^t$ and $e_2 = (0 \quad 1)^t$. Let ψ, ϕ be the linear maps from the standard simplex to the simplices Δ_1 and Δ_2 such that

$$\psi(e_i) = g_i,\ \phi(e_i) = h_i \text{ for } i = 0, 1, 2.$$

Then f is the composition $f(p) = \psi(\phi^{-1}(p))$. Define

$$v_1 = g_1 - g_0\ v_2 = g_2 - g_0$$

and without loss of generality assume they are linearly independent. $\phi : \mathbb{R}^2 \to \mathbb{R}^n$ is still a multi-dimensional map, but the image of ϕ is a two-dimensional plane $H \in \mathbb{R}^n$. Therefore it is possible to choose an orthonormal basis $(b_1, \ldots, b_n)$ for $\mathbb{R}^n$ such that H is spanned by b_1 and b_2 and $b_1 = \frac{v_1}{\|v_1\|}$. With this basis it suffices to explain ϕ on the first two dimensions

$$\begin{aligned} v_1 &= \|v_1\| \cdot b_1 \\ v_2 &= \|v_2\| \cdot R_{angle(v1,v2)} \cdot b_1, \end{aligned}$$

where $R_\alpha = \begin{pmatrix} \cos\alpha & -\sin\alpha \\ \sin\alpha & \cos\alpha \end{pmatrix}$ is the two-dimensional rotation matrix for the reduced basis b_1, b_2. So v_2 can be represented as

$$v_2 = \|v_2\| \cdot \begin{pmatrix} \frac{\langle v_1, v_2\rangle}{\|v_1\|\cdot\|v_2\|} \\ \sqrt{1 - \left(\frac{\langle v_1, v_2\rangle}{\|v_1\|\cdot\|v_2\|}\right)^2} \end{pmatrix}.$$

$\partial\phi$ represents the corresponding matrix to the reduced basis

$$\partial\phi = \begin{pmatrix} \|v_1\| & \frac{\langle v_1, v_2\rangle}{\|v_1\|} \\ 0 & \|v_2\| \cdot \sqrt{1 - \left(\frac{\langle v_1, v_2\rangle}{\|v_1\| \cdot \|v_2\|}\right)^2} \end{pmatrix}$$

and

$$\begin{aligned} &(\partial\phi)^t \cdot \partial\phi \\ &= \begin{pmatrix} \|v_1\| & 0 \\ \frac{\langle v_1, v_2\rangle}{\|v_1\|} & \|v_2\| \cdot \sqrt{1 - \left(\frac{\langle v_1, v_2\rangle}{\|v_1\| \cdot \|v_2\|}\right)^2} \end{pmatrix} \cdot \begin{pmatrix} \|v_1\| & \frac{\langle v_1, v_2\rangle}{\|v_1\|} \\ 0 & \|v_2\| \cdot \sqrt{1 - \left(\frac{\langle v_1, v_2\rangle}{\|v_1\| \cdot \|v_2\|}\right)^2} \end{pmatrix} \\ &= \begin{pmatrix} \|v_1\|^2 & \langle v_1, v_2\rangle \\ \langle v_1, v_2\rangle & \|v_2\|^2 \end{pmatrix} \end{aligned}$$

and $\det \partial\phi = \sqrt{\|v_1\|^2 \cdot \|v_2\|^2 - \langle v_1, v_2\rangle^2} = \|v_1 \wedge v_2\|$ by Lagrange's identity. Analogously for ψ:

$$(\partial\psi)^t \cdot \partial\psi = \begin{pmatrix} \|w_1\|^2 & \langle w_1, w_2\rangle \\ \langle w_1, w_2\rangle & \|w_2\|^2 \end{pmatrix}$$

Shift the order of the matrices in the trace computation since $tr(A \cdot B) = tr(B \cdot A)$ and apply some further basic matrix-calculation rules to compute the trace of $\partial f^t \partial f$

$$\begin{aligned} &tr((\partial f)^t \cdot \partial f) \\ &\quad = tr((\partial\phi^{-1})^t \cdot (\partial\psi)^t \cdot \partial\psi \cdot \partial\phi^{-1}) \\ &\quad = tr((\partial\psi)^t \cdot \partial\psi \cdot \partial\phi^{-1} \cdot (\partial\phi^{-1})^t) \\ &\quad = tr((\partial\psi)^t \cdot \partial\psi \cdot ((\partial\phi)^t \cdot \partial\phi)^{-1}) \\ &\quad = \begin{pmatrix} \|v_1\|^2 & \langle v_1, v_2\rangle \\ \langle v_1, v_2\rangle & \|v_2\|^2 \end{pmatrix} \cdot \begin{pmatrix} \|w_1\|^2 & \langle w_1, w_2\rangle \\ \langle w_1, w_2\rangle & \|w_2\|^2 \end{pmatrix}^{-1} \\ &\quad = \frac{1}{(det\partial\phi)^2} \begin{pmatrix} \|v_1\|^2 & \langle v_1, v_2\rangle \\ \langle v_1, v_2\rangle & \|v_2\|^2 \end{pmatrix} \cdot \begin{pmatrix} \|w_2\|^2 & -\langle w_1, w_2\rangle \\ -\langle w_1, w_2\rangle & \|w_1\|^2 \end{pmatrix} \\ &\quad = \frac{1}{(det\partial\phi)^2} \left(\langle v_1, v_1\rangle \cdot \langle w_2, w_2\rangle - 2\langle v_1, v_2\rangle \cdot \langle w_1, w_2\rangle + \langle v_2, v_2\rangle \cdot \langle w_1, w_1\rangle\right). \end{aligned}$$

Using the substitution $v_3 := v_2 - v_1$ and therefore $-2\langle v_1, v_2\rangle = \|v_3\|^2 - \|v_1\|^2 - \|v_2\|^2$ yields

$$\begin{aligned}
&tr((\partial f)^t \cdot \partial f)\\
&\quad = \frac{1}{(det\partial\phi)^2}\left(\|v_1\|^2\langle w_2, w_2\rangle + (\|v_3\|^2 - \|v_1\|^2 - \|v_2\|^2)\langle w_1, w_2\rangle + \|v_2\|^2\langle w_1, w_1\rangle\right)\\
&\quad = \frac{1}{(det\partial\phi)^2}\left(\|v_1\|^2\langle w_2 - w_1, w_2\rangle + \|v_3\|^2\langle w_1, w_2\rangle + \|v_2\|^2\langle w_1 - w_2, w_1\rangle\right)\\
&\quad = \frac{1}{(det\partial\phi)}\left(\|v_1\|^2\frac{\langle w_2 - w_1, w_2\rangle}{(det\partial\phi)} + \|v_3\|^2\frac{\langle w_1, w_2\rangle}{(det\partial\phi)} + \|v_2\|^2\frac{\langle w_1 - w_2, w_1\rangle}{(det\partial\phi)}\right).
\end{aligned}$$

Since $\cot(\alpha) = \frac{\cos(\alpha)}{\sin(\alpha)}$ and

$$\begin{aligned}
\cos(angle(w_1, w_2)) &= \frac{\langle w_1, w_2\rangle}{\|w_1\| \cdot \|w_2\|}\\
\sin(angle(w_1, w_2)) &= \frac{\|w_1 \wedge w_2\|}{\|w_1\| \cdot \|w_2\|}
\end{aligned}$$

it follows that $\frac{\langle w_1, w_2\rangle}{det\partial\phi} = cot(angle(w_1, w_2))$. Additionally,

$$\|(w_2 - w_1) \wedge w_2)\| = \|(w_1 - w_2) \wedge w_1)\| = \|(w_1) \wedge w_2)\|$$

shows that $\frac{\langle (w_2 - w_1), w_2\rangle}{det\partial\phi} = cot(angle(w_2 - w_1, w_2)$ and $\frac{\langle (w_1 - w_2), w_1\rangle}{det\partial\phi} = cot(angle(w_1 - w_2, w_1)$ or in the shorter notation $\alpha_1, \alpha_2, \alpha_3$ and a_1, a_2, a_3 as figure 4.1 indicates

$$tr((\partial f)^t \cdot \partial f) = \frac{1}{det\partial\phi}\sum_{i=1}^{3}\cot(\alpha_i) \cdot a_i^2.$$

Now the Dirichlet energy can be computed as

$$\begin{aligned}
E_D(f) =& \frac{1}{2}\int_{\Delta_1} tr((\partial f)^t \partial f)\\
=& \frac{1}{2}\int_{\Delta_e} tr((\partial f)^t \partial f)(det\partial\phi)\\
=& \frac{1}{2}\int_{\Delta_e} \frac{1}{det\partial\phi}\sum_{i=1}^{3}\cot(\alpha_i) \cdot a_i^2 (det\partial\phi)\\
=& \frac{1}{2}\sum_{i=1}^{3}\cot(\alpha_i) \cdot a_i^2 \int_{\Delta_e} 1\\
=& \frac{1}{4}\sum_{i=1}^{3}\cot(\alpha_i) \cdot a_i^2.
\end{aligned}$$

□

Remark Pinkall and Polthier showed this in [PP93] for simplicial complexes Σ_g in $\mathbb{R}^m$ and Σ_h in $\mathbb{R}^n$ with (possibly) different metrics g on $\mathbb{R}^m$ and h on $\mathbb{R}^n$. Then the norms and scalar-products in the proof of 4.5 have to be modified to $\|.\|_h$ and $\|.\|_g$ but the result stays the same with respect to the different metric. That means that the angles α_i are computed with the help of g and the lengths a_i with the help of h.

Application to Riemannian Manifolds

The question arises wheter this works in a Riemannian manifold, too.

The abstract simplicial complex is independent of the embedding space and only specifies the number of vertices and the connectivity of the vertices. Therefore, definition 4.1 in the Euclidean setting extends to a discrete structure for a surface in $\mathcal{M}$. To make it easier to cope with maps and the energy formula, here it is additionally required, that all triangles are unique geodesic triangles. That means that when the points p_1, p_2, $p_3 \in \mathcal{M}$ form the triangle Δ in the simplicial complex Σ, there is a chart $\phi : U \to \mathbb{R}^m$ with $p_1, p_2, p_3 \in U$ and all points in U can be uniquely connected by geodesics.
For two geodesic triangles Δ_g and Δ_h in two Riemannian manifolds $(\mathcal{M}, g)$ and $(\mathcal{N}, h)$ with (possibly) different Riemannian metrics g and h a map $f : \Delta_g \to \Delta_h$ induced by the vertices can be extended to a linear map on the interior by local coordinates. Let the points $(p_1, p_2, p_3) \subset U \subset \mathcal{M}$ be the vertices of Δ_g and $(q_1, q_2, q_3) \subset V \subset \mathcal{N}$ be the vertices of Δ_h with the charts (ϕ, U) and (ψ, V) specified as before, then $\psi \circ f \circ \phi^{-1} : \mathbb{R}^m \to \mathbb{R}^n$ is a map as in the Euclidean setting 4.3 with different induced metrics. Since f is constructed by map on single triangles the energy formula (4.6) is valid if the triangulation is fine enough which means that all triangles in the triangulation are geodesic triangles.

4.2 Algorithm of Pinkall and Polthier

The previous theorem 4.5 showed that the Dirichlet energy depends only on the angles in the domain triangulation and the lengths in the image triangulation. Typically, to minimize the Dirichlet energy a map $f : D \to \Sigma$ from a triangulation of the unit disk D in $\mathbb{R}^2$ to the discrete surface Σ in the manifold $\mathcal{M}$ is minimized. Therefore, a triangulation of D would be needed. A conformal reparametrisation would then change the domain triangulation of the disk. Pinkall and Polthier proposed to take the map $f : \Sigma_i \to \Sigma$ from one discrete surface Σ_i in $\mathcal{M}$ to the next discrete surface $f(\Sigma_i) = \Sigma$ to avoid this two-step algorithm.

Definition 4.6 (Plateau's Problem, Discrete)**.** *Let $\Gamma = (\Gamma_1, \ldots, \Gamma_N)$ be the boundary points and Σ_0 an initial discrete surface where the boundary points coincide with Γ. The goal is to find a discrete locally area-minimizing surface Σ in the set of all*

discrete surfaces of the same simplicial complex type and with the same boundary points.

$$\mathcal{S} = \{\Sigma \mid \Sigma \textit{ is a simplicial two-complex with fixed boundary and of the same type as } \Sigma_0\} \tag{4.7}$$

Algorithm 1 contains the pseudo code of the algorithm of Pinkall and Polthier. Step 3 needs to solve an minimization problem in each step. As initial data for the

Algorithm 1 Minimal Surface

1: Take Σ_0 as the initial discrete surface Σ, set i to 0.
2: **repeat**
3: Compute Σ_{i+1} as the minimum $\min_\Sigma \frac{1}{2} \int_{\Sigma_i} |\nabla f : \Sigma_i \to \Sigma|^2$.
4: Set $\Sigma_{i+1} := \Sigma$ and i to $i + 1$.
5: **until** $|A(\Sigma_{i-1}) - A(\Sigma_i)| < \varepsilon$

minimization $f := id_{\Sigma_i}$ is used. In step 5 $A(\Sigma_i) = E_D(id_{\Sigma_i})$ can be used for the area computation, since id_{Σ_i} is harmonic and conformal.

Hierarchical Algorithm

The distance approximations for the shape spaces are only locally valid, which means that the elements must be close enough. Consequently, the discrete surface is only a good approximation to a continuous surface if the triangulation is fine enough. The degree of the refinement needed depends on the shape space and the distance approximation. Therefore, the algorithm was modified to an adaptive, hierarchical algorithm to validate the granularity of the refinement. That means that the algorithm of Pinkall and Polthier is repeatedly applied for triangulations with increasing number of vertices. For each refinement the outcome of the algorithm is used as input and then a new optimisation step is done. The convergence of this outer loop means that the discrete surface is a good approximation for the continuous surface.

Algorithm 2 Hierarchical Minimal Surface

1: Take an initial triangulation $\Sigma_{0,0}$ as the initial Σ , set i and j to 0.
2: **repeat**
3: **repeat**
4: Compute Σ_{i+1} as the minimum $\min_\Sigma \frac{1}{2} \int_{\Sigma_i} |\nabla f : \Sigma_i \to M|^2$.
5: Set i to $i + 1$.
6: **until** $|A(\Sigma_{j,i}) - A(\Sigma_{j,i-1})| < \varepsilon$
7: Refine the simplicial complex of $\Sigma_{i,j}$.
8: Set i to 0 and j to $j + 1$.
9: **until** $|A(\Sigma_{j,0}) - A(\Sigma_{j-1,0})| < \varepsilon$

Algorithm 2 shows the modified version of the algorithm. Step 3 to 5 correspond to the original algorithm 1. Step 2 starts an outer loop which contains the refinement process.

In the case where the surface lies in $\mathbb{R}^3$ with the standard metric, [PP93] provides a convergence theorem.

Theorem 4.7. *The algorithm 1 converges in $\mathbb{R}^n$ with the Euclidean metric to a discrete surface as solution of Plateau's problem 4.6 if no triangle degenerates during the minimization.*

Proof. The proof can be divided into three steps.

1. The algorithm constructs a sequence (Σ_i, f_i) with decreasing area.
2. The space of all possible triangulations is compact which implies that there exists a converging minimal subsequence.
3. The limit has zero Dirichlet energy derivative.

The main key of the proof is the compactness in item 2. In the hope to generalize this to Riemannian manifolds this is done very detailed in this thesis despite the fact that this was omitted in [PP93].

Step 1 The sequence of $\{\Sigma_i, f_i\}$ provided by the algorithm has decreasing area, since

$$\begin{aligned} A(\Sigma_i) = E_D(id|_{\Sigma_i}) &\geq E_D(f_i : \Sigma_i \to \Sigma_{i+1}) \\ &\geq E_D(id|_{\Sigma_{i+1}}) = A(\Sigma_{i+1}). \end{aligned}$$

Step 2 Let $\mathcal{S}_{pos} \subset \mathcal{S}$ denote the set of all non-degenerating discrete surfaces with the same boundary and the same simplicial complex type. The compactness is shown in the following corollary 4.10. Assume for now, that the space is compact, then there exists a subsequence Σ_i converging uniformly to a limit surface Σ.

Step 3 Show for the sequence $\Sigma_i \to \Sigma$, that Σ is a critical point of the Dirichlet energy.
For $\mathcal{S}_{pos}$ as in Step 2 with $\|.\|$ the product topology as induced topology define F_i as

$$\begin{aligned} F_i :&\mathcal{M} \to \mathbb{R} \\ &X \mapsto E_D(f_i : \Sigma_i \to X). \end{aligned}$$

In the Euclidean setting, F_i is quadratic and has a minimum in Σ_{i+1}, i.e.

$$\nabla F_i|_{\Sigma_{i+1}} = 0.$$

Because $\mathcal{S}_{pos}$ is compact, there is a uniform bound s_{max} on the norm of $\nabla^2 f_i$ independent of i. That means that by the mean value theorem

$$\nabla F_i|_{\Sigma_i} = \nabla F_i|_{\Sigma_i} - \nabla F_i|_{\Sigma_{i+1}} = \nabla^2 F_i|_\xi |\Sigma_i - \Sigma_{i+1}|^2$$

and with the uniform bound

$$\nabla F_i|_{\Sigma_i} \leq s_{max} |\Sigma_i - \Sigma_{i+1}|^2.$$

Since $\Sigma_i \to \Sigma$ it follows for the limit $F_i \to F_\Sigma$ that $\nabla F_\Sigma|_\Sigma = 0$. That means that Σ is a critical point of the energy function $E_D(f_i : \Sigma \to X)$. □

The compactness of $\mathcal{S}_{pos}$ is an important aspect of the proof, since it is needed to extract a converging subsequence and to get a uniform bound. Pinkall and Polthier did not explain what they meant by non-degenerating, however, the requirement is that during the process no angles should degenerate. So it should also be avoided that angles converge to 0 or π. Therefore an ε-criterion for the non-degeneracy is introduced. For a triangle with vertices x_1, x_2, and x_3 and corresponding angles α_1, α_2, and α_3 non-degeneracy with respect to $\tilde{\varepsilon} > 0$ or $\varepsilon > 0$ means that for all angles

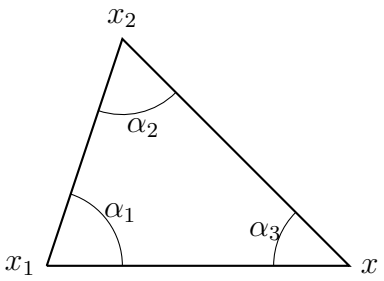

$$0 + \tilde{\varepsilon} \leq \alpha_i \leq \pi - \tilde{\varepsilon} \text{ for } i = 1, 2, 3$$

or

$$-1 + \varepsilon \leq \cos \alpha_i \leq 1 - \varepsilon \text{ for } i = 1, 2, 3. \tag{4.8}$$

Take

$$\mathcal{S}^\varepsilon_{pos} := \mathcal{S} \cap \{\Sigma \text{ simplicial two-complex} \mid \text{ all } \Delta_i \text{ have no } \varepsilon\text{-degenerated angles}\}$$

as the set of all possible discrete surfaces. Drop the ε if the exact value is not relevant, as in theorem 4.7. The compactness of $\mathcal{S}^\varepsilon_{pos}$ is shown step-by-step, first in lemma 4.8 for triangles with two fixed vertices, then in corollary 4.9 for triangles with one fixed vertex and finally for a generic simplicial complex as in corollary 4.10.

Lemma 4.8. *Given $x_1, x_2 \in \mathbb{R}^n$ such that $x_1 \neq x_2$ then*

$$\mathcal{S}^\varepsilon(x_1, x_2) := \{x \in \mathbb{R}^n \mid (x_1, x_2, x) \text{ spans a triangle where no angle is } \varepsilon\text{-degenerated } \} \tag{4.9}$$

is a closed subset of $\mathbb{R}^n$ and bounded w.r.t. $\|.\|_2$, hence, compact.

Proof. Need to show that $S^\varepsilon(x_1, x_2)$ is closed and bounded.

Show that $S^\varepsilon(x_1, x_2)$ is closed: The non degenerate condition can be formulated with

$$F(x) = \begin{pmatrix} \cos\alpha_1 \\ \cos\alpha_2 \\ \cos\alpha_3 \end{pmatrix} = \begin{pmatrix} \frac{\|x_2-x\|^2+\|x_1-x\|^2-\|x_2-x_1\|^2}{2\|x_2-x\|\cdot\|x_1-x\|} \\ \frac{\|x_2-x_1\|^2+\|x_1-x\|^2-\|x_2-x\|^2}{2\|x_2-x_1\|\cdot\|x_1-x\|} \\ \frac{\|x_2-x\|^2+\|x_2-x_1\|^2-\|x_1-x\|^2}{2\|x_2-x\|\cdot\|x_2-x_1\|} \end{pmatrix}$$

$$x \in \mathcal{S}^\varepsilon(x_1, x_2) \Leftrightarrow F(x) \subset [-1+\varepsilon, 1-\varepsilon]^3. \tag{4.10}$$

The condition that the sum $\alpha_1 + \alpha_2 + \alpha_3 = \pi$ is automatically satisfied, if equation 4.10 is satisfied. $F : \mathbb{R}^n \to \mathbb{R}^3$ is continuous for all $x \in \mathbb{R}^n \backslash \{x_1, x_2\}$. Since $[-1+\varepsilon, 1-\varepsilon]^3 \subset \mathbb{R}^3$ is a closed subset, the preimage $F^{-1}(\{[-1+\varepsilon, 1-\varepsilon]^3\})$ is also closed.

Show that $S^\varepsilon(x_1, x_2)$ is bounded: Assume $\mathcal{S}^\varepsilon(x_1, x_2)$ is unbounded, then there exists a sequence $(x^k)_{k\in\mathbb{N}} \subset \mathcal{S}^\varepsilon(x_1, x_2)$ such that $\|x^k\| \xrightarrow{k\to\infty} \infty$. W.l.o.g. $x_1 = 0$. Then

$$\begin{aligned} cos(\alpha_3) &= \frac{\|x_2 - x^k\|^2 + \|x^k\|^2 - \|x_2\|^2}{2\|x_2 - x^k\| \cdot \|x^k\|} \\ &\underbrace{\geq}_{a\cdot b \leq \frac{a^2+b^2}{2}} \frac{\|x_2 - x^k\|^2 + \|x^k\|^2 - \|x_2\|^2}{\|x_2 - x^k\|^2 + \|x^k\|^2} \\ &= 1 - \underbrace{\frac{\|x_2\|^2}{\|x_2 - x^k\|^2 + \|x^k\|^2}}_{\xrightarrow{k\to\infty} 0} \end{aligned}$$

gets arbitrarily close to one, i.e. the angle α_3 degenerates. Therefore, $\mathcal{S}^\varepsilon(x_1, x_2)$ is bounded. □

The next step is a similar result for a triangle, where one point is fixed and another point lies in a compact subset. Here it follows that again the set of all such triangles is compact.

Corollary 4.9. *Let $K \subset \mathbb{R}^d$ be compact and $x_1 \in \mathbb{R}^d$, then*

$$\mathcal{S}^\varepsilon(x_1, K) := \{(x, y) \in \mathbb{R}^{2\cdot d} \mid x \in K,\ y \in \mathcal{S}^\varepsilon(x_1, x)\} \tag{4.11}$$

is compact.

Proof. The set is bounded, because K and $\mathcal{S}^\varepsilon(x_1, x)$ are compact.
For the closedness, let x_k, y_k be a converging sequence in $\mathcal{S}^\varepsilon(x_1, K)$ with

$$(x_k, y_k) \xrightarrow{k\to\infty} (x, y)$$

with respect to the product topology. Then $x \in K$ since K is compact. It remains to show that $y \in \mathcal{S}^\varepsilon(x_1, x)$. Since the condition 4.10 is satisfied for all y_k and x_k corresponding to x and x_2 in terms of condition 4.10, the limits for each term exist and the divisors are $\neq 0$. Therefore, this condition is also satisfied for $k \to \infty$. □

The proof works for subsets

$$\{(x, y, z) \in \mathbb{R}^{n\cdot d} \mid x \in K_1, y \in K_2,\ z \in \mathcal{S}^\varepsilon(x, y)\}$$

and compact sets K_1 and K_2 with an analogous argumentation.

Corollary 4.10.

$$\mathcal{S}^\varepsilon_{pos} := \mathcal{S} \cap \{\Sigma \textit{ simplicial two-complex} \mid \textit{ all } \Delta_i \textit{ have no } \varepsilon\textit{-degenerated angles}\}$$

is compact.

Proof. This is proven by induction over the number of interior points. For a fixed set $\Gamma = (\Gamma_1, \ldots, \Gamma_N)$ of boundary vertices and a fixed abstract simplicial complex define

$$\mathcal{S}^\varepsilon_k := \{(y_1, \ldots, y_k) \in (\mathbb{R}^n)^k \mid \text{where } (y_1, \ldots, y_k) \text{ are the inner vertices and no triangle is } \varepsilon\text{-degenerated.}\}$$

as the set of all possible discrete surfaces.

Base Case $k = 1$**:** Since there is only one interior vertex, all triangles of the simplicial complex have at least two fixed vertices. Therefore, $\mathcal{S}^\varepsilon_1$ is the intersection of finitely many $\mathcal{S}^\varepsilon(\Gamma_i, \Gamma_j)$ and is, hence, compact.

Inductive Step $k \to k + 1$**:** Assume $\mathcal{S}^\varepsilon_k$ is a compact set for a fixed boundary set Γ and all simplicial complexes with k inner vertices. Let Σ_{k+1} be an arbitrary simplicial complex for the boundary Γ and $k + 1$ inner vertices, then there exists a simplicial complex Σ_k such that Σ_{k+1} emerges from Σ_k by adding an interior vertex and a finite number of triangles $\{\Delta_1, \ldots, \Delta_Q\}$. Since $\mathcal{S}^\varepsilon_k$ is compact for all types of simplicial complexes with k interior vertices, for all triangles Δ_i at least two vertices lie in compact sets. Therefore, $\mathcal{S}^\varepsilon_{k+1} = \mathcal{S}^\varepsilon_k \times \cap \mathcal{S}^\varepsilon(K_i, K_j)$ is compact again as a finite intersection of compact sets times a compact set. □

Figure 4.2 shows an example where the new simplicial complex specified by the 5 interior vertices $\{p_1, p_2, p_3, p_4, q\}$ emerges from the simplicial complex with 4 interior vertices $\{p_1, p_2, p_3, p_4\}$ and adding the missing four triangles.

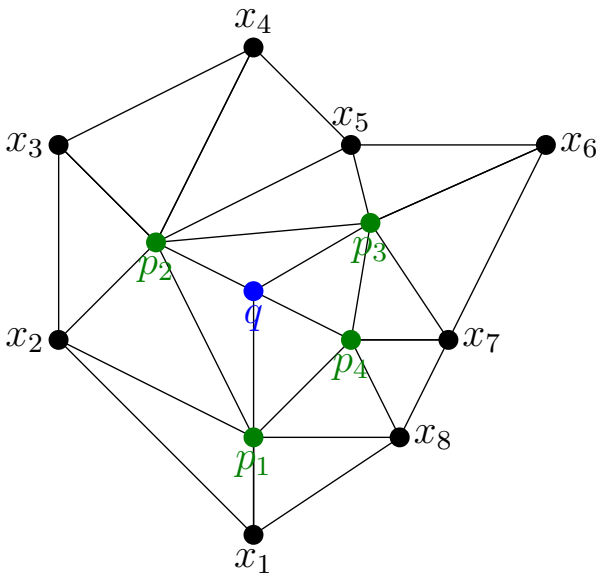

Figure 4.2: An example triangulation for 8 fixed outer points and 5 interior points.

4.3 Implementation

In this section the main ideas of the implementation are explained.
To get the code running see the supplied "Readme.md" in the code-archive of the enclosed CD. The algorithm was implemented due to efficiency in C. Besides the standard libraries, *GSL*[1], *LAPACK*[2] and *OpenMP*[3] are needed, gcc[4] v. 4.9.2 was used to compile the source code. GSL is the gnu scientific library and includes a BGFS-method[5] which is used for the optimisation step. Alternatively, in the Euclidean case, LAPACK is used to solve linear equations for the exact solution. OpenMP is used to parallelize the computations. That is not necessary but gives a considerable speedup. To visualise the shape spaces and create plots gnuplot[6], paraview[7] and tikz[8] were used. These are, however, not necessary to run the program. The code I wrote can roughly be divided into four parts:

1. Discrete Geodesic Calculus
   This is needed for the boundary computation in shape spaces.

[1] `http://www.gnu.org/software/gsl/`
[2] `http://www.netlib.org/lapack/`
[3] `http://openmp.org/`
[4] `https://gcc.gnu.org/`
[5] Broyden-Fletcher-Goldfarb-Shanno algorithm, a quasi-Newton optimisation method
[6] `http://www.gnuplot.info/`
[7] `http://www.paraview.org/`
[8] `https://www.ctan.org/pkg/pgf`

2. Minimal Surface
   For the minimal surface computation, the energy computation is implemented as in theorem 4.5.

3. Distance Approximations
   Different underlying spaces were used for the energy computations, so an abstraction to the distance approximation was implemented. A shape space is then represented by points in $\mathbb{R}^{k\cdot d}$ and a map $\mathbb{R}^{k\cdot d} \times \mathbb{R}^{k\cdot d} \to \mathbb{R}$.

4. Triangulation
   The discrete surfaces are represented by triangulations.

Discrete Geodesics

The discrete geodesic calculus part is an implementation of section 2.2. Given a shape space with a distance approximation, two points in the shape space and the length of the discrete curve, the algorithm computes a discrete geodesic γ connecting these two points. This is solved by directly minimizing the energy $E(\gamma) = K \cdot \sum_i W(\gamma_i, \gamma_{i+1})$ with a BFGS-method supplied by GSL.

Minimal Surfaces

The minimal surface part is in principal the same as the discrete geodesic part, since it implements the Dirichlet energy and then uses again BFGS for minimizition. To compute the energy of a triangulation Σ the formula

$$E_D(\Sigma) = \sum_{\Delta\in\Sigma} E_D(\Delta) = \sum_{\Delta\in\Sigma} \frac{1}{4} \sum_{i=1}^{3} \cot \alpha_i^\tau |a_i^\tau|_n^2 \tag{4.12}$$

is used. The angle α_i was computed with help of the law of cosine

$$\cos \alpha_i = \frac{b^2 + c^2 - a^2}{2 \cdot b \cdot c} \tag{4.13}$$

where a, b and c are the corresponding lengths of edges, computed by the distance

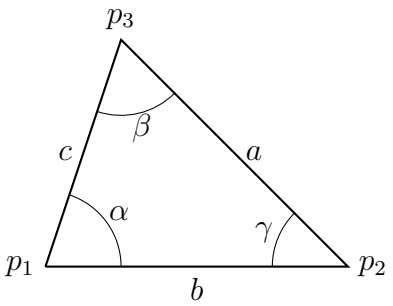

approximation. Let the triangle Δ for which the integral is computed have the

vertex points p_1, p_2 and p_3 and lengths $a = \sqrt{W(p_2, p_3)}$, $b = \sqrt{W(p_3, p_1)}$, and $c = \sqrt{W(p_1, p_2)}$. This performs badly for a rough triangulation, but the closer the points in $\mathcal{M}$ the better is the Euclidean approximation to the actual geodesic triangle. Therefore, assume that the triangulation is fine enough so that this gives a good angle approximation. In the Euclidean case if a triangle is degenerated, i.e. an angle is less than $0°$ or greater than $180°$, then all angles are degenerated. Since here the angles are computed with the formula

$$\cos^{-1} \frac{a^2 + b^2 - c^2}{2ab} \tag{4.14}$$

the angle is degenerated if

$$\frac{a^2 + b^2 - c^2}{2ab} \leq -1$$

or

$$\frac{a^2 + b^2 - c^2}{2ab} \geq 1.$$

Therefore, the previous statement is still true.

Lemma 4.11. *The non-degeneracy condition is equivalent to the three triangle inequalities for the distances of the points p_1, p_2 and p_3*

$$-1 < \frac{a^2 + b^2 - c^2}{2ab} < 1$$

$$\Leftrightarrow a + b - c > 0 \quad \wedge \quad +a - b + c > 0 \quad \wedge \quad -a + b + c > 0$$

Proof. Since $a, b, c > 0$, a short calculation shows this.

$$\begin{aligned}
& -1 < \frac{a^2 + b^2 - c^2}{2ab} < 1 \\
\Leftrightarrow\ & -2ab < a^2 + b^2 - c^2 < 2ab \\
\Leftrightarrow\ & -(a+b)^2 < -c^2 \quad \wedge \quad (a-b)^2 < c^2 \\
\underbrace{\Leftrightarrow}_{a,b,c>0}\ & a + b > c \quad \wedge \quad |a - b| < c \\
\Leftrightarrow\ & c < a + b \quad \wedge \quad a - b < c \quad \wedge \quad b - a < c \\
\Leftrightarrow\ & c < a + b \quad \wedge \quad a < c + b \quad \wedge \quad b < c + a
\end{aligned}$$

□

These inequalities also implies that $\alpha_1 + \alpha_2 + \alpha_3 = \pi$ since the angles of a Euclidean triangle sum up to pi. Furthermore, if these inequalities are satisfied, the Dirichlet energy $E_D(id_{\Sigma_i} : \Sigma_i \to M)$ is positive, and has another representation depending only on the lengths.

Theorem 4.12.

$$E_D(f : \Delta_1 \to \Delta_2) = \frac{1}{4}(\cot\alpha_1 \cdot a_2^2 + \cot\beta_1 \cdot b_2^2 + \cot\gamma_1 \cdot c_2^2)$$

where α_1 corresponds to the opposite angle of a_1 in the domain triangle and a_2 is the length in the image triangle, analogously for β_2, b_2, γ_2 and c_2. This can be simplified to

$$E_D(id_\Delta) = \frac{1}{4}\frac{a_2^2(b_1^2+c_1^2-a_1^2) + b_2^2(a_1^2+c_1^2-b_1^2) + c_2^2(a_1^2+b_1^2-c_1^2)}{\sqrt{(-(a_1^4+b_1^4+c_1^4) + 2\cdot(a_1^2b_1^2+b_1^2c_1^2+c_1^2a_1^2))}}. \tag{4.15}$$

When f is the identity id_Δ which means that the domain triangle and image triangle coincide the previous equations simplify to

$$E_D(id_\Delta) = \frac{1}{4}\sqrt{(-(a^4+b^4+c^4) + 2\cdot(a^2b^2+b^2c^2+c^2a^2))}. \tag{4.16}$$

Proof. Let Δ_1 and Δ_2 be defined by the lengths (a_1, b_1, c_1) and (a_2, b_2, c_2), respectively, let $(\alpha_1, \beta_1, \gamma_1)$ denote the induced angles in Δ_1. Consider

$$\cot(\cos^{-1}(s)) = \frac{s}{\sqrt{1-s^2}}$$

then

$$\begin{aligned}
a_2^2 \cdot \cot(\alpha_1) &= a_2^2 \cdot \cot(\cos^{-1}\left(\frac{b_1^2+c_1^2-a_1^2}{2b_1c_1}\right)) \\
&= \frac{a_2^2(b_1^2+c_1^2-a_1^2)}{2b_1c_1} \cdot \left(\sqrt{1-\left(\frac{b_1^2+c_1^2-a_1^2}{2b_1c_1}\right)^2}\right)^{-1} \\
&= a_2^2(b_1^2+c_1^2-a_1^2)\left(\sqrt{-(a_1^4+b_1^4+c_1^4)+2(a_1^2b_1^2+b_1^2c_1^2+c_1^2a_1^2)}\right)^{-1}.
\end{aligned}$$

Computing $a_2^2 \cdot \cot(\alpha_1) + b_2^2 \cdot \cot(\beta_1) + c_2^2 \cdot \cot(\gamma_1)$ proves (4.15).
The second equation follows from a calculation in the numerator of (4.15) with $a := a_1 = a_2$, $b := b_1 = b_2$ and $c := c_1 = c_2$. The numerator computes as

$$\begin{aligned}
a^2(b^2+c^2-a^2) + b^2(a^2+c^2-b^2) + c^2(a^2+b^2-c^2) \\
= -(a^4+b^4+c^4) + 2(a^2b^2+b^2c^2+c^2a^2).
\end{aligned}$$

and this is the square of the denominator. So it proves (4.16). □

Remarks

1. In the Euclidean setting, the degeneracy of a triangle is equivalent to two lengths adding up to the third, e.g. $a = b + c$. (4.16) shows that then the Dirichlet energy $E_D(\Delta) = 0$ which implies that the impact of degenerated triangles on the Dirichlet energy of a triangulation is non-negative.

2. An interesting fact for shape spaces is based on $\cot\alpha > 0$ for all angles $0 < \alpha < \pi/2$. Therefore, when the initial triangle is acute, the Dirichlet energy is positive, independent of the lengths in the image triangle. This applies also to distance approximations which are neither symmetric, positive definite nor satisfy the triangle inequality.

Distance Approximations

The main key to implementing a shape space is to provide the squared distance approximation. Therefore, every formula, where a distance is required, was reformulated, such that $W(\ ,\ )$ is used. For the BGFS-methods additionally the distance derivatives were needed.

Triangulation

To represent the surfaces or geodesics, a triangulation was implemented. It can be specified by a set of points and a connectivity matrix. To compute the Dirichlet energy only the triangulation and distance approximation are needed. The triangulation can be saved to and read from a vtk file to make it compatible with paraview in the three-dimensional setting.
To implement the hierarchical algorithm mentioned in 4.2 a refinement method was implemented. One of the most simple refinements is splitting each existing triangle into four new triangles by creating new vertices in the middle of each edge and connecting those.

(a) Initial 3 point triangulation.

(b) After one refinement step.

Figure 4.3: Visualisation of the refinement method.

This refinement method behaves better than the more naive refinement which is achieved by simply adding the centroid and three edges connecting the old vertices with the centroid. Since in the used refinement method there are always less than or equal to 6 triangles at all vertices of the refinement if the initial triangulation satisfies this property. This is not valid in the case of adding the centroid.

The number of vertices v, edges e and connections t depends on the initial triangulation and can be computed with the help of

$$\begin{aligned} v(n) &= v(n-1) + e(n-1) \\ e(n) &= 2 \cdot e(n-1) + 3 \cdot t(n-1) \\ t(n) &= 4 \cdot t(n-1) = 4^{n-1} \cdot t_0. \end{aligned}$$

Or by solving the recursive definitions

$$\begin{aligned} v(n) &= v_0 + \frac{1}{4}(2^n - 1)(4e_0 + (2^{n+1} - 1)t_0) = v_0 + \mathcal{O}(2^n)e_0 + \mathcal{O}(2^{2n})t_0 \qquad (4.17) \\ e(n) &= 2^{n-3}(4 \cdot e_o + 3(2^n - 1)t_0) = \mathcal{O}(2^{2n})t_0 + \mathcal{O}(2^n)e_0 \\ t(n) &= 4^{n-1} \cdot t_0 = \mathcal{O}(2^n)t_0. \end{aligned}$$

Equation (4.17) shows that the number of vertices is exponential in the number of refinement steps. That is why in most cases only up to 10 refinement steps were computed.
During the refinement new shapes have to be computed. Ideally, these shapes would be computed with the help of discrete geodesics since the new points should lie in the middle of an edge. Since for each edge a discrete geodesic would have to be computed this is way too expensive. For example a triangulation with 6 initial triangles has, after 5 refinement steps, 3169 vertices and 6144 edges. Therefore, the midpoints are computed by an Euclidean averaging of the $\mathbb{R}^n$ representation of those shapes.
For an initial triangulation in a shape space there is still missing a method to compute initial data. In the case of discrete geodesics it is possible to take 0 as initial data, not so in the case of discrete minimal surfaces, since the used algorithm always needs non degenerated angles.
In the experiments two initialisation methods were evaluated.

1. By choosing the origin and orientation as shown in the chapter 2.3, one could simply compute an Euclidean interpolation.

2. By setting all the interior points to an edge vertex and performing first a step of a different algorithm to minimize the energy.

The algorithm of the second case, to minimize the Dirichlet energy, is not based on Pinkall and Polthier's algorithm, but instead minimizes directly the energy of the map $f : D \to M$ from the unit disk in $\mathbb{R}^2$ into the manifold. This can be computed with the help of algorithm 1 by setting the angles of the start manifold to the angles of a triangulation of the unit disk.

5 Examples

The algorithm was tested first on some simple examples to evaluate its behaviour and then applied to shape spaces. The pictures were created with gnuplotb, paraview and tikz.

5.1 Euclidean Space

The first example is a validation for the algorithm, the second example shows that the algorithm works in a slightly more complex setting. Furthermore, two different initialisations for the interior vertices of the minimal surfaces are tested and compared.

5.1.1 Standard Metric

The first case is the typical problem of Plateau which means that, for a boundary curve Γ in $\mathbb{R}^3$ with the standard metric which bounds at least one surface of finite area, find a surface of least area bounded by this curve. In this setting theorem 3.8 ensures that a minimal surface exists and theorem 4.7 shows that the algorithm 1 converges to such a minimal surface. With this algorithm it also is possible to compute minimal surfaces bounded by multiple boundary curves, however, in this thesis only minimal surfaces of disk-type are computed.

The boundary curve is given by a set of points $\{x_1, \dots, x_n\} \subset \mathbb{R}^3$ which discretize a simple closed curve. As distance the standard distance $d^2(x, y) = \|x - y\|_2^2$ is used. Therefore, the Dirichlet energy is a quadratic problem and there is an exact solution in each step of algorithm 1. The smooth sinus-like curve

$$\Gamma(t) = \begin{pmatrix} \sin(2 \cdot \pi \cdot t) \\ \cos(2 \cdot \pi \cdot t) \\ -1 + \sin^2(2 \cdot \pi \cdot t) \end{pmatrix}$$

is used in the following test cases as boundary.

Exact Solution

Figure 5.1 shows a side and top view of the resulting surface computed by the algorithm. This discrete surface looks like it approximates a smooth surface and could describe a soap-film bounded by a wire.

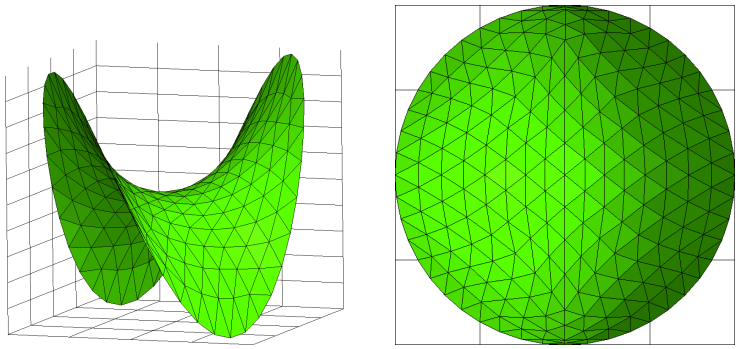

(a) side-view (b) top-view

Figure 5.1: A discrete minimal surface in $\mathbb{R}^3$ with a sinus-like boundary curve. The triangulation consists of 384 triangles and 217 vertices.

Since in this case the standard metric is used, the Dirichlet energy is a quadratic function and there is an exact form for the solution (see [PP93]). Figure 5.2 shows the Dirichlet energy and number of points over the iterate count where the exact solution is used in each step. Each coloured segment encodes a refinement, the

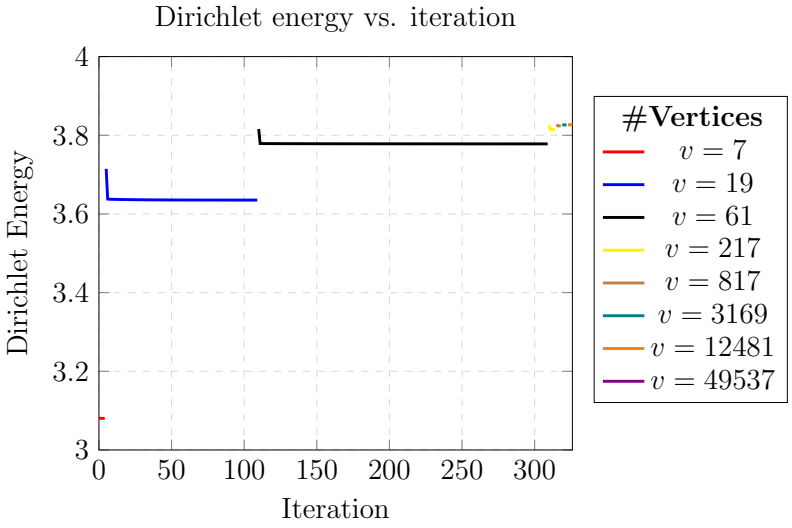

Figure 5.2: Convergence graph for the hierarchical algorithm 2 in the Euclidean setting with exact solutions in each step. The Dirichlet energy is plotted versus the number of algorithm, the colour encodes the refinement.

number of vertices is given in the legend. This configuration starts with 6 outer vertices and one inner vertex and an optimum for the Dirichlet energy is reached after only a few steps. Since in this granularity the optimum is reached, the triangulation is refined and a new optimization process is started. The new Dirichlet energy for 19 vertices varies a lot from the earlier one. After only one step the energy is close to the optimum with 19 vertices, but it takes some time to converge.

This is qualitatively the same for the refinement with 61 vertices. For even finer triangulations the energy does not vary that much after a refinement and it takes fewer optimisation steps for a fixed refinement.
This shows that the algorithm behaves as expected. There is a convergence for each refinement and there is even an overall convergence. Furthermore, for a fixed refinement the convergence looks interesting since after a few steps the Dirichlet energy is close to the optimum but it takes a lot of steps to finally converge, this was also observed in [PP93].

Approximated Solution

In a general setting the minimization of the Dirichlet energy requires an optimisation algorithm. For this, a quasi-Newton optimisation algorithm is used. The c-library GSL provides an implementation of a BFGS[1]-method and, as a validation, this was also tested in the standard Euclidean case. Figure 5.3 shows the graph for the same setting as before but with an optimisation step instead of the exact solution. Both,

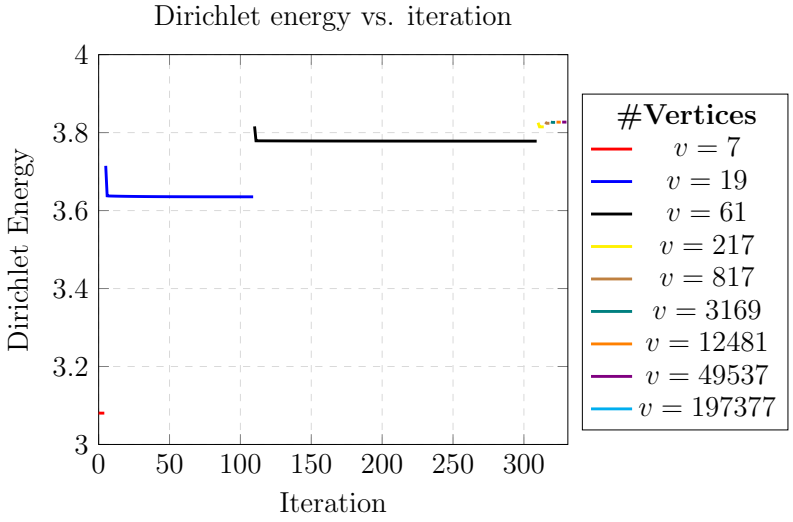

Figure 5.3: Convergence graph for the hierarchical algorithm 2 in the Euclidean setting, computing the minimum by a BFGS-method in each step. The Dirichlet energy is plotted against the number of iteration steps, the colour encodes the refinement.

the exact and the BFGS method, achieve the same values for the Dirichlet energy in all cases where both can compute a solution. However, the exact method needs a system of linear equations to be solved and the used algorithm to solve linear equations fails if the triangulation has too many interior points.

[1]Broyden-Fletcher-Goldfarb-Shanno algorithm

Initial Simplicial Complex

The used triangulation not only influences the type of surface but also influences the conformality of the surface. In figure 5.4 four different initial simplicial complexes are compared. There are only slight differences in the Euclidean setting, however, a bad initial simplicial complex leads to bad artifacts in the more complex cases.

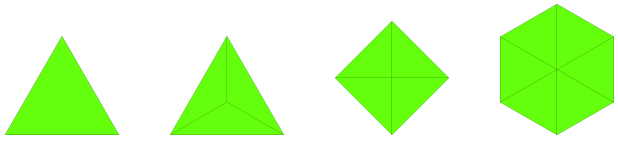

(a) 1 triangle (b) 3 triangles (c) 4 triangles (d) 6 triangles

Figure 5.4: Four different types of initial simplicial complexes.

Figure 5.5 shows the discrete surfaces for the different initial simplicial complexes. This shows that the conformality depends on the initial triangulation. However, table 5.1 shows that the Dirichlet energies are close for highly refined triangulations.

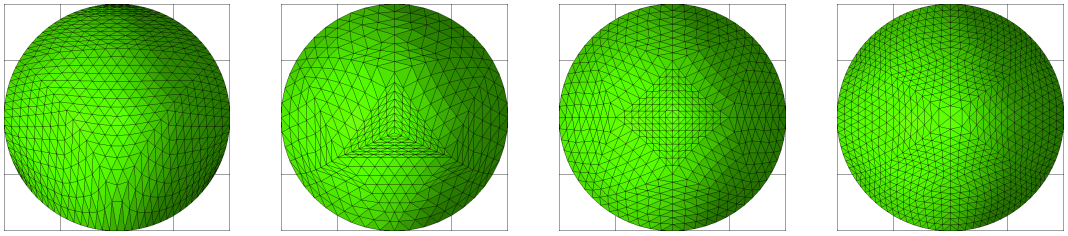

(a) 465 inner vertices and $E_D = 5.288$. (b) 361 inner vertices and $E_D = 5.269$ (c) 481 inner vertices and $E_D = 5.28$. (d) 721 inner vertices and $E_D = 5.285$.

Figure 5.5: Discrete minimial surfaces for the same boundary curve and four different initial simplicial comlexes.

Initialisation

The interior vertices of the discrete surface need an initialisation. In an Euclidean setting an arithmetic average can be easily computed, but this fails or is expensive in more complicated settings. Therefore, an additional method for the initialisation in the Euclidean setting was tested. The idea of the additional algorithm, denoted be disk-minimization algorithm, is to minimize the Dirichlet energy of the map $f : D \to M$ for a fixed triangulation of the unit disk $D \subset \mathbb{R}^2$. This ignores the conformality condition, but does not require non-degenerated triangles in the initial discrete surface. Therefore, the interior points can all be set to one of the boundary points. The minimizer of this Dirichlet energy can be computed with the help of algorithm 1 with D as the initial surface. That means that the initial angles are all

Table 5.1: Performance of the algorithm in the Euclidean setting with different initial simplicial complexes.

Simplicial Complex	Refinement	E_D	#Vertices	#Interior
t1	3	5.268100357	45	21
t1	4	5.285079522	153	105
t1	5	5.288472731	561	465
t1	6	5.289197269	2145	1953
t3	3	5.207916545	109	85
t3	4	5.269204511	409	361
t3	5	5.284385311	1585	1489
t3	6	5.288155516	6241	6049
t4	3	5.253207633	256	113
t4	4	5.280781112	545	481
t4	5	5.287193087	2113	1985
t4	6	5.288857261	8321	8065
t6	3	5.274307712	217	169
t6	4	5.285678166	817	721
t6	5	5.288479064	3169	2977
t6	6	5.289184153	12481	12097

set to the same value, e.g. to $\frac{\pi}{3}$.

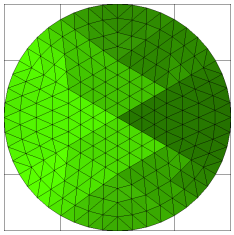

Figure 5.6: Initial triangulation with an Euclidean averaging as initialisation step with 217 vertices.

Figure 5.6 shows the initialisation of the triangulation for 217 vertices. This triangulation is achieved as described in section 4.3. This explains the edges in the figure, however, the Dirichlet energy for this surface is still close to the optimum (see table 5.2). An advantage of this initialisation is that it is easy and fast to compute when it is possible to compute it.
In figure 5.4 the triangulation for the disk-minimizer algorithm is shown. Here the same simplicial complex as in the Euclidean averaging is used but all interior vertices are set to one (arbitrary) boundary point. The triangulation after the initialisation step (fig 5.7 (b)) is already close to the optimum.

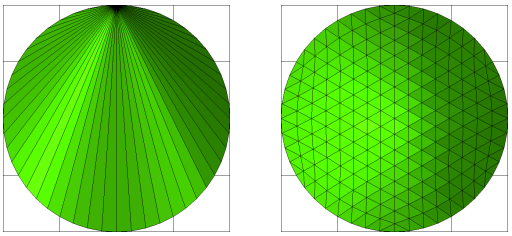

(a) Pre init (b) Post init

Figure 5.7: Triangulation before and after the initialisation.

Table 5.2: Performance of the algorithm in the Euclidean setting with different initialisation methods.

Initialisation	E_D Initialisation	E_D Optimisation	#Vertices	#Interior
Euclidean	4.181745	4.181745	7	1
Euclidean	5.276228	4.995270	19	7
Euclidean	5.583723	5.212980	61	37
Euclidean	5.661445	5.270553	217	169
disk-min $\pi/3$	4.181745	4.181745	7	1
disk-min $\pi/3$	5.027355	4.995271	19	7
disk-min $\pi/3$	5.253754	5.212971	61	37
disk-min $\pi/3$	5.310858	5.270344	217	169

Table 5.2 shows the Dirichlet energy after the initialisation step and after the convergence for that refinement. The optimum for the additional initialisation step is slightly lower than with the Euclidean averaging.

5.1.2 Distorted Metric

The second case uses a slightly more complex distance function and tries to evaluate whether this algorithm could work in Riemannian manifolds. The setting is basically the same as before, Γ describes a discrete simple and closed curve in $\mathbb{R}^n$, but now the distance is distorted by effects motivated by gravity. This means that instead of the Euclidean distance a distance approximation is used that is defined as the squared standard distance multiplied with a positive function $f : \mathbb{R} \to \mathbb{R}^{>0}$.

$$W(x, y) = f(\|x\|) \cdot \|x - y\|^2 \tag{5.1}$$

For the following computations $f(t) = \varepsilon + \sigma \cdot (t - \delta)^\eta$ with $\varepsilon = 1$, $\sigma = 1$, $\delta = 1$ and $\eta = 2$ is used.
The derivatives of $W(x, y)$ are

$$\begin{aligned}\frac{\partial}{\partial x} W(x,y) &= \frac{\partial}{\partial x} f(\|x\|) \cdot \|x - y\|^2 + f(\|x\|) \cdot \frac{\partial}{\partial x} \|x - y\|^2 \\ &= \sigma \cdot \eta \cdot (\|x\| - \delta)^{\eta - 1} \frac{x}{\|x\|} \cdot \|x - y\|^2 \\ &+ 2 \cdot f(\|x\|)(x - y)\end{aligned}$$

and

$$\frac{\partial}{\partial y} W(x,y) = -2 f(\|x\|) \cdot (x - y).$$

The motivation for this example is that a sphere S^2 is embedded as usual in $\mathbb{R}^3$ and it is cheaper to walk on the surface of the sphere than to travel through the sphere or the orbit.

The boundary curve is again a smooth curve sampled at some points. Here, as boundary curve, a flat circle Γ

$$\Gamma(t) = \begin{pmatrix} r \cdot \sin(2 \cdot \pi \cdot t) \\ r \cdot \cos(2 \cdot \pi \cdot t) \\ z_0 \end{pmatrix}$$

is used which is shifted in the z-coordinate by z_0. In the first example z_0 is slightly above the xy-plane, in the second example z_0 is greater than the radius of the sphere and r controls the radius of the boundary curve.
Figure 5.8 shows the discrete minimal surface for $z_0 = 0.01$. With the standard metric the minimal surface of such a curve would be the disk bounded by this curve. In the image the surface avoids the origin and has a bump towards the distorting sphere.

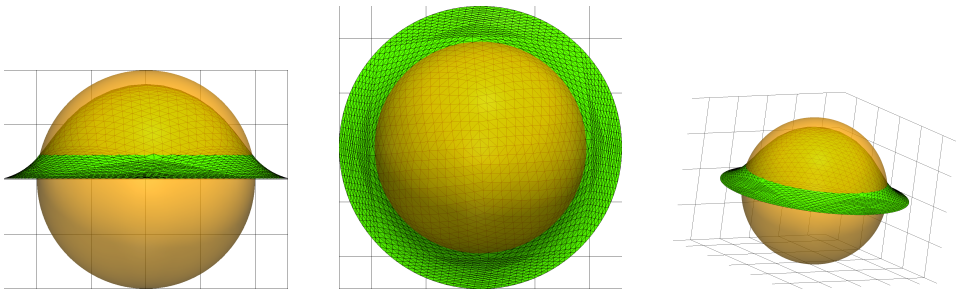

Figure 5.8: Three different views of the discrete minimal surface with a distorted metric and transparent sphere. The boundary has a shift $z_0 = 0.01$.

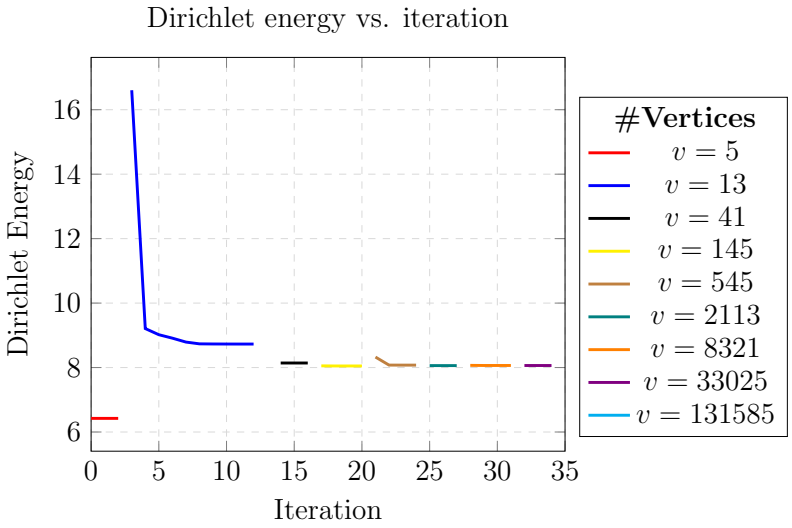

Figure 5.9: Number of Iteration vs Dirichlet Energy of the iteration steps for the distorted Euclidean setting with a shift $z_0 = 0.01$ and radius $r = 1$.

Figure 5.11 shows the discrete minimal surface for $z_0 = 2$ and radius $r = 2$. Here again, the discrete minimal surface is no planar disk but has a bump towards the sphere.
As the graphs 5.9 and 5.10 show, the algorithm converges for both boundary curves.

Initial Simplicial Complex

In the standard Euclidean setting the impact of the different initial simplicial complexes was little. In this distorted case, however, for some initial triangulations the discrete surface degenerated during the algorithm (see figure 5.12). This happened for the initial simplicial complex with 6 triangles. Normally this is a good triangulation because in combination with the used refinement each interior vertex always has 6 surrounding triangles.
For the initial examples (figures 5.8 and 5.11) the initial simplicial complex with four initial triangles was used.

Initialisation

In the case of a distorted metric, not only the initial triangulation, but also the initialisation has a much greater impact since the Euclidean average is a bad approximation. Table 5.3 compares the Euclidean average to the disk-minimizer initialisation.
For the same refinement and initial simplicial complex the Dirichlet energy after the initialisation differs a lot. The triangulation achieved by the disk-minimizer is already close to the optimum whereas the Euclidean average is a lot worse. Furthermore, the optimal values differ.

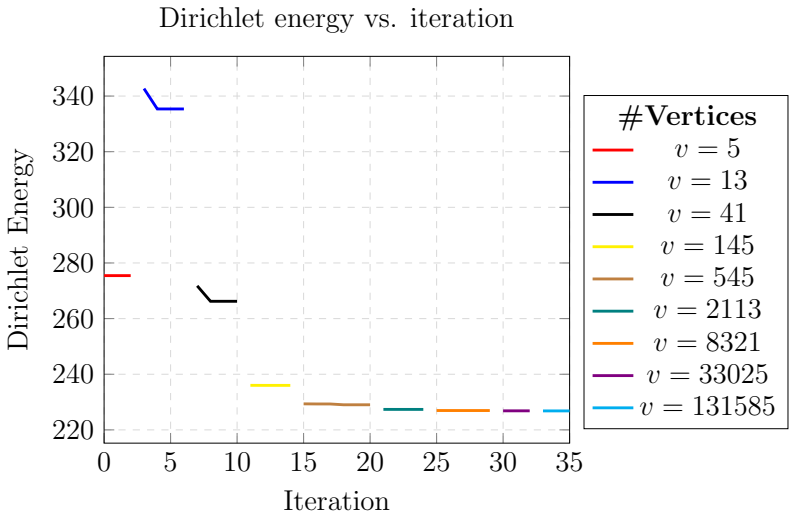

Figure 5.10: Number of Iterations vs Dirichlet Energy of the iteration steps for the distorted Euclidean setting with a shift $z_0 = 2$ and radius $r = 2$.

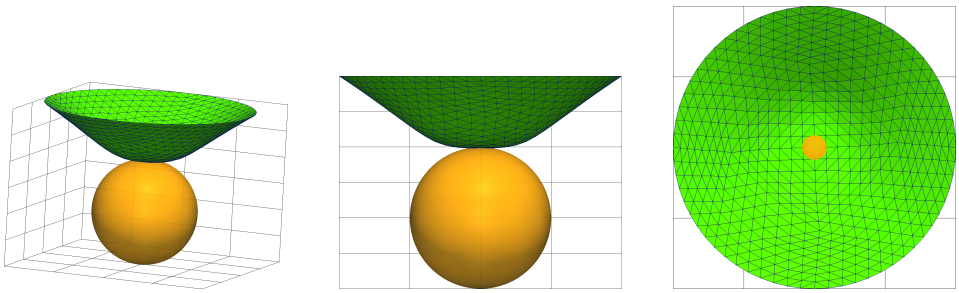

Figure 5.11: Three different views of the discrete minimal surface with a distorted metric and transparent sphere. The boundary is above the sphere.

5.2 Shape Spaces: Finite Viscous Rods

This section considers shape spaces as defined in section 3.3. These are more complicated than the Euclidean space with the distorted metric from before. The elements of the shape spaces are approximated by finite piecewise jointed straight wires. The distance approximation is motivated by the physical energy it would take to bend and stretch one such wire into another. There are two different representations either for an open or a closed rod, where the open setting is more simple and provides the basis for the closed setting. For a more detailed introduction to viscous rods see [RW15].

5.2.1 Visualisation

Since discrete minimal surfaces in shape spaces are generally not embeddable in $\mathbb{R}^2$ or $\mathbb{R}^3$ the visualisation is trickier. However, each point of the shape spaces can be

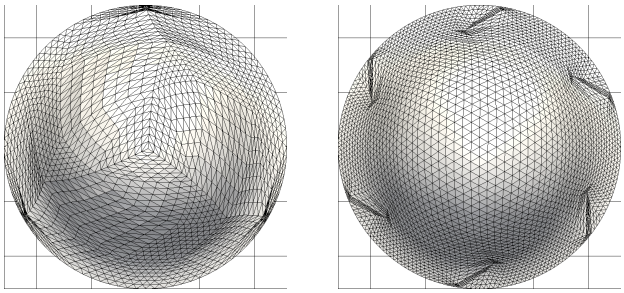

Figure 5.12: Discrete minimal surfaces for two different initial complexes. Here no angles are degnerated, however, the triangulation has varying triangles with some close to degenerated.

Table 5.3: Distorted metric setting with two different initialisation methods.

Initialisation	E_D Initialisation	E_D Optimisation	#Vertices	#Interior
Euclidean	11.214788	8.055520	817	721
Euclidean	11.230132	8.060863	3169	2977
disk-min $\pi/3$	8.059823	8.057655	817	721
disk-min $\pi/3$	8.063619	8.061419	3169	2977

printed in $\mathbb{R}^2$ and the structure of the triangulation is independent of the shape space. One way to visualize a discrete minimal surface is by printing each object on a grid defined by the abstract simplicial complex. Figure 5.13 shows two examples for such grids. The advantage of this method is that even for higher refinements the indices stay the same. That means that, even after a refinement step, the same shapes can easily be plotted.

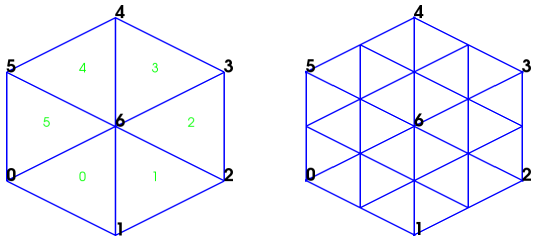

Figure 5.13: Two grids for printing a minimal surface with 7 and 19 initial points

During the computation of discrete minimal surfaces in shape spaces it often occurs that triangles degenerate. Therefore, another visualisation of the discrete surface is computed. This second visualisation is based again on the grid of the triangulation and the fact that the discrete surface is approximated by Euclidean triangles. This means that the three vertices of a triangle in the shape space induce three length a, b and c and these can in turn induce a triangle in $\mathbb{R}^2$ which is used to compute the angles for the Dirichlet energy. These approximated Euclidean triangles are printed

within the grid as figure 5.14 shows. For all triangles the same scale factor was used such that the relative lengths can be compared.

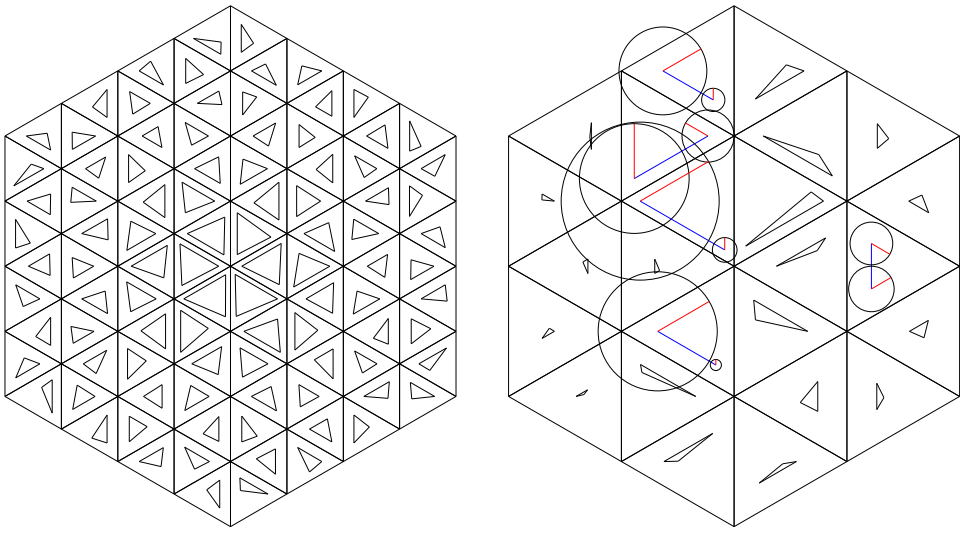

(a) Distorted Euclidean space (b) Shape space

Figure 5.14: A visualisation of the approximated triangles for two different settings. (b) has degenerated triangles.

In a setting with a symmetric distance approximation the common edge of two adjacent triangles has the same length. However, in the distorted Euclidean space and the shape spaces this is not necessarily the case. Figure 5.14 (b) shows an example where triangles are degenerated. The plotted circles show that there is no triangle with the edge lengths induced by the vertices. More technically, the lengths a, b and c correspond to a triangle in $\mathbb{R}^2$ if and only if $a + b > c$, $a + c > b$ and $b + c > a$.

5.2.2 Open Viscous Rods

Approximation of the Distance

An open finite viscous rod is represented by a list of n lengths and $n - 1$ angles.

$$\gamma = (l_1, \ldots, l_n, \alpha_1, \ldots, \alpha_{n-1}) \tag{5.2}$$

For two such rods γ and β the distance is approximated by

$$W_{open}(\gamma, \beta) = \sum_{i=1}^{n} \frac{(l_i^\gamma - l_i^\beta)^2}{l_i^\gamma} + \frac{1}{2} \sum_{i=1}^{n-1} \frac{(\alpha_i^\gamma - \alpha_i^\beta)^2}{l_i^\gamma + l_{i+1}^\gamma} \tag{5.3}$$

with derivatives

$$\begin{aligned}
\frac{\partial}{\partial l_k^\gamma} W_{open}(\gamma,\beta) =& 1 - \left(\frac{l_k^\beta}{l_k^\gamma}\right)^2 - \frac{1}{2}\left(\frac{(\alpha_{k-1}^\gamma - \alpha_{k-1}^\beta)^2}{(l_{k-1}^\gamma + l_k^\gamma)^2} + \frac{(\alpha_k^\gamma - \alpha_k^\beta)^2}{(l_k^\gamma + l_{k+1}^\gamma)^2}\right) \\
\frac{\partial}{\partial \alpha_k^\gamma} W_{open}(\gamma,\beta) =& \frac{\alpha_k^\gamma - \alpha_k^\beta}{l_k^\gamma + l_{k+1}^\gamma} \\
\frac{\partial}{\partial l_k^\beta} W_{open}(\gamma,\beta) =& -2 + 2\frac{l_k^\beta}{l_k^\gamma} \\
\frac{\partial}{\partial \alpha_k^\beta} W_{open}(\gamma,\beta) =& -\frac{\alpha_k^\gamma - \alpha_k^\beta}{l_k^\gamma + l_{k+1}^\gamma}.
\end{aligned}$$

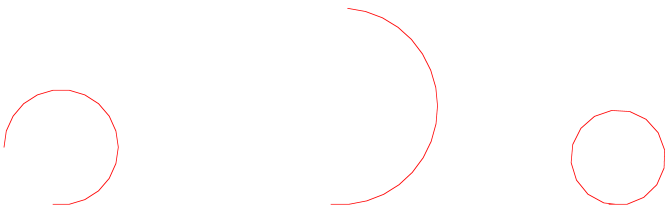

(a) p_1 (b) p_2 (c) p_3

Figure 5.15: Three open viscous rods which are close to each other.

Boundary Curve

The boundary curve of the shape space examples consists of three given rods which are connected by geodesics. Note that this curve is not even smooth anymore. Here the initial rods can be seen in figure 5.15 and are very close to each other (approximated distance from p_1 to p_2 it is 0.00567, from p_2 to p_3 it is 0.00582, and from p_3 to p_1 it is 0.00571).

Minimal Surface

The metric for the open and closed viscous rods is a lot more complicated and, additionally, the distance approximation is not symmetric. This makes the computation of discrete minimal surfaces more complicated and, therefore, fails very often due to degenerated triangles. The first example consists of three initial rods with respect to the metric approximation and shows that it is possible for the algorithm to find a discrete minimal surface locally. The initial interior points are taken as the Euclidean average of the lengths and angles. Figure 5.16 (a) shows the resulting discrete surface and the graph in figure 5.17 shows that the algorithm converges. In this example no angles degenerate during the minimisation process.

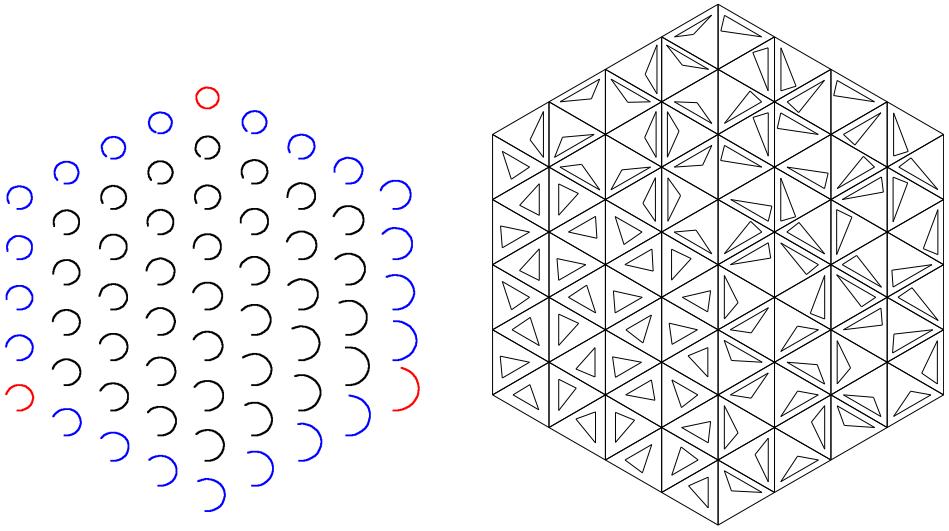

(a) Discrete Minimal Surface (b) Approximated Euclidean Triangles

Figure 5.16: Open viscous rods with close initial data.

In figure 5.18 (a) the red shapes mark the three initial given points. In blue are the discrete geodesics connecting these three points and in black are the interior points of the discrete minimal surface drawn. Here the initial simplicial complex with 6 triangles is used.

5.2.3 Closed Viscous Rods

A closed finite viscous rod is usually represented by the coordinates, which specify the joints of the wire. The energy is still based on lengths and angles, so a transformation is needed, which makes the functional more complicated. This approach, however, makes it easy to handle the requirement of closedness.

Derivatives of the Distance Approximation

A closed finite viscous rod is represented by a list of n points in $\mathbb{R}^2$. Implemented as $x \in \mathbb{R}^{2n}$.

$$x = (x_1, \dots, x_n) \in (\mathbb{R}^2)^n$$

The approximation to the distance is computed as the composition

$$W_{closed}(x, y) = W(P(x), P(y)), \tag{5.4}$$

where $P : (\mathbb{R}^2)^n \longrightarrow (\mathbb{R}^n)^2$ is the mapping which transforms the coordinates in lengths and angles and $W : (R^n)^2 \times (\mathbb{R}^n)^2 \longrightarrow \mathbb{R}^{\geq 0}$ is a modified version of the distance for non-closed finite viscious rods as in the previous chapter.
To simplify the derivatives and avoid too many cases, assume $-1 = n - 1$, $0 = n$, $n + 1 = 1$ and so on.

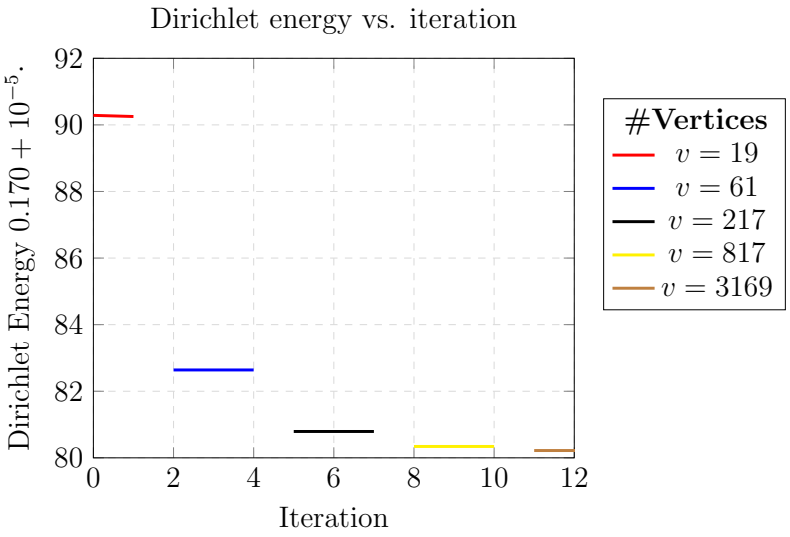

Figure 5.17: Convergence graph for open viscous rods.

Modified Energy Let $\gamma = (l_1^\gamma, \dots, l_n^\gamma, \alpha_1^\gamma, \dots, \alpha_n^\gamma)$ and $\beta = (l_1^\beta, \dots, l_n^\beta, \alpha_1^\beta, \dots, \alpha_n^\beta)$ be the lengths and angles representation. Then the distance approximation is defined as

$$W(\gamma, \beta) = \sum_{i=1}^{n} \frac{(l_i^\gamma - l_i^\beta)^2}{l_i^\gamma} + 2 \sum_{i=1}^{n} \frac{(\alpha_i^\gamma - \alpha_i^\beta)^2}{l_i^\gamma + l_{i+1}^\gamma}. \tag{5.5}$$

Lengths and Angles The length part is pretty simple, for the angles some additional computations are needed.

$$P(x) = P(x_1, \dots, x_n) = (\|x_1 - x_2\|, \dots, \|x_{n-1} - x_n\|, \|x_n - x_1\|, \tag{5.6}$$
$$\theta_{x_2}(x_1, x_3), \theta_{x_3}(x_2, x_4), \dots, \theta_{x_{n-1}}(x_{n-2}, x_n), \theta_{x_n}(x_{n-1}, x_1), \theta_{x_1}(x_n, x_2)) \tag{5.7}$$

The maps $\theta_q(v, w) : \mathbb{R}^2 \times \mathbb{R}^2 \times \mathbb{R}^2 \longrightarrow [0, 2\pi]$ compute the clockwise oriented angle between the vectors $v - q$ and $w - q$

$$\bar{\theta}_q(v, w) := \cos^{-1} \frac{\langle v - q, w - q \rangle}{\|v - q\| \cdot \|w - q\|} \tag{5.8}$$

and

$$\theta_q(v, w) = \begin{cases} \bar{\theta}_q(v, w) & \text{if } \langle (v - q)^\perp, (w - q) \rangle \leq 0 \\ 2\pi - \bar{\theta}_q(v, w) & \text{if } \langle (v - q)^\perp, (w - q) \rangle > 0 \end{cases} \tag{5.9}$$

for $y = (y_1, y_2)$ is $y^\perp = (y_2, -y_1)$.

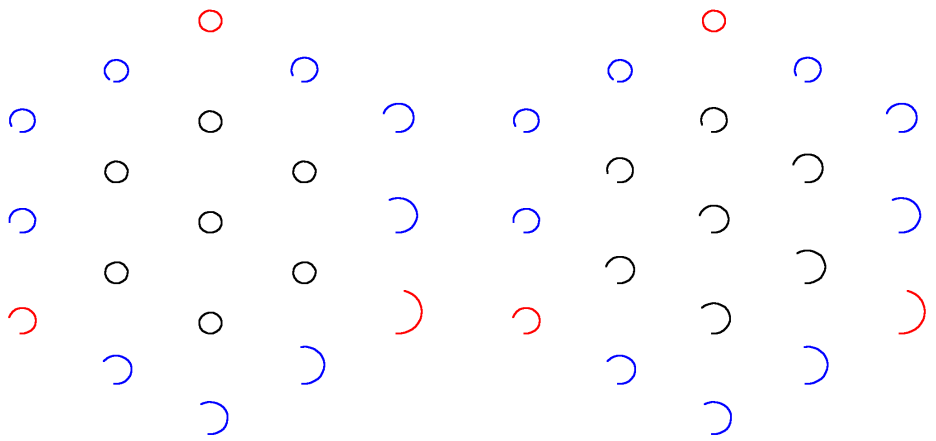

(a) Pre Initialisation (b) Post Initialisation

Figure 5.18: Open viscous rods with badly initialised data

Derivatives For the BFGSmethod the first derivatives of W_{closed} are needed. The following paragraph gives the derivatives of the single functions and the derivatives of W_{closed} are computed with the help of chain rule.

$$\frac{\partial}{\partial v}\bar{\theta}_q(v,w) = \frac{1}{\sqrt{1-\left(\frac{\langle v-q,w-q\rangle}{\|v-q\|\cdot\|w-q\|}\right)^2}}\left(\frac{\langle v-q,w-q\rangle(v-q)}{\|v-q\|^3\|w-q\|} - \frac{w-q}{\|v-q\|\cdot\|w-q\|}\right)$$

$$\frac{\partial}{\partial w}\bar{\theta}_q(v,w) = \frac{1}{\sqrt{1-\left(\frac{\langle v-q,w-q\rangle}{\|v-q\|\cdot\|w-q\|}\right)^2}}\left(\frac{\langle v-q,w-q\rangle(w-q)}{\|w-q\|^3\|v-q\|} - \frac{v-q}{\|v-q\|\cdot\|w-q\|}\right)$$

$$\frac{\partial}{\partial q}\bar{\theta}_q(v,w) = -\frac{1}{\sqrt{1-\left(\frac{\langle v-q,w-q\rangle}{\|v-q\|\cdot\|w-q\|}\right)^2}}\cdot$$
$$\left(\frac{2q-(v-w)}{\|v-q\|\cdot\|w-q\|} + \langle v-q,w-q\rangle\left(\frac{v-q}{\|v-q\|^3\cdot\|w-q\|} + \frac{w-q}{\|v-q\|\cdot\|w-q\|^3}\right)\right)$$

and thus

$$\frac{\partial}{\partial v}\theta_q(v,w) = \begin{cases} \frac{\partial}{\partial v}\bar{\theta}_q(v,w) & \text{if } \langle (v-q)^\perp, w-q\rangle \le 0 \\ -\frac{\partial}{\partial v}\bar{\theta}_q(v,w) & \text{otherwise.} \end{cases}$$

The derivatives $\frac{\partial}{\partial w}$ and $\frac{\partial}{\partial q}$ can be computed analogously. The partial derivative of $P(x)$ is

$$\begin{aligned}\frac{\partial}{\partial x_k}P(x_1,\dots,x_n) = \\ \Bigg(0,\dots,0,-\frac{x_{k-1}-x_k}{\|x_{k-1}-x_k\|},\frac{x_k-x_{k+1}}{\|x_k-x_{k+1}\|},0,\dots,0, \\ 0,\dots,\frac{\partial}{\partial x_k}\theta_{x_{k-1}}(x_{k-2},x_k),\frac{\partial}{\partial x_k}\theta_{x_k}(x_{k-1},x_{k+1}),\frac{\partial}{\partial x_k}\theta_{x_{k+1}}(x_k,x_{k+2}),\dots,0\Bigg).\end{aligned}$$

Here it suffices to know 5 entries so this problem does not increase with n. The total derivative of $W(\gamma,\beta) = W((l_1^\gamma,\dots,l_n^\gamma,\alpha_1^\gamma,\dots,\alpha_n^\gamma),(l_1^\beta,\dots,l_n^\beta,\alpha_1^\beta,\dots,\alpha_n^\beta))$ is

$$\begin{aligned}\frac{\partial}{\partial l_k^\gamma}W(\gamma,\beta) &= 1-\left(\frac{l_k^\beta}{l_k^\gamma}\right)^2-2\left(\frac{(\alpha_{k-1}^\gamma-\alpha_{k-1}^\beta)^2}{(l_{k-1}^\gamma+l_k^\gamma)^2}+\frac{(\alpha_k^\gamma-\alpha_k^\beta)^2}{(l_k^\gamma+l_{k+1}^\gamma)^2}\right)\\ \frac{\partial}{\partial \alpha_k^\gamma}W(\gamma,\beta) &= \frac{(\alpha_k^\gamma-\alpha_k^\beta)}{l_k^\gamma+l_{k+1}^\gamma}\\ \frac{\partial}{\partial l_k^\beta}W(\gamma,\beta) &= -2+2\frac{l_k^\beta}{l_k^\gamma}\\ \frac{\partial}{\partial \alpha_k^\beta}W(\gamma,\beta) &= -\frac{(\alpha_k^\gamma-\alpha_k^\beta)}{l_k^\gamma+l_{k+1}^\gamma}.\end{aligned}$$

Collecting all these cases leads to

$$\frac{\partial}{\partial x_k}W(P(x),P(y)) = W_1(P(x),P(y))\cdot\frac{\partial}{\partial x_k}P(x) \tag{5.10}$$

$$\frac{\partial}{\partial y_k}W(P(x),P(y)) = W_2(P(x),P(y))\cdot\frac{\partial}{\partial y_k}P(x). \tag{5.11}$$

Note that since $\frac{\partial}{\partial y_k}P(x)$ is zero except for 5 entries, only these 5 entries are computed for W_1 and W_2.

Boundary Curve

In this setting similar to the open rods the three initial points from figure 5.19 are given and used as input for the algorithm.

Minimal Surface

These are not as close as in the open viscous rod case but with a proper initial simplicial complex and initialisation a discrete minimal surface can be computed. These points, however, are further apart, the approximate distances of these shapes are, from p_1 to p_2 1.0170, p_2 to p_3 1.0861 and p_3 to p_1 1.0045. Figure 5.20 shows

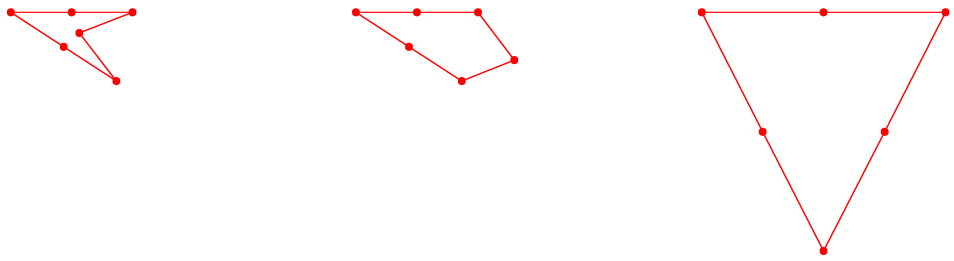

(a) p_1 (b) p_1 (c) p_1

Figure 5.19: Closed viscous rods

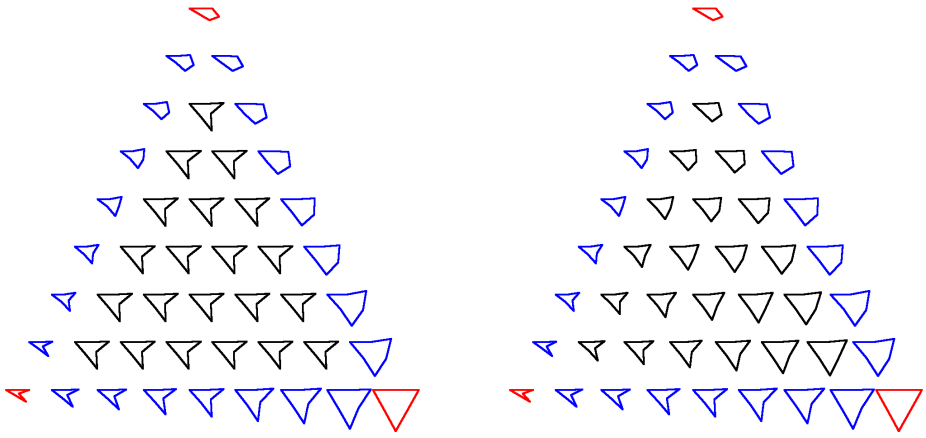

(a) Pre Initialisation (b) Post Initialisation

Figure 5.20: Discrete surfaces pre and post an initialisation step for closed viscous rods with badly initialised data

the discrete minimal surface, here again with the initialisation step. It is possible to work again with an Euclidean averaging of the coordinates of the closed viscous rods, however, in general this approach is more interesting. The convergence graph, see figure 5.21, shows that in this configuration the algorithm converges as well, until even by refinement no better optimum is achieved. This is due to the fact, that during the process of the algorithm in this configuration no angles degenerate. When starting with a different initial simplicial complex this does not work as well. In figure 5.22 the approximated Euclidean triangles can be seen. This shows the triangles with 45 vertices right before the first refinement step. In comparison to different initial simplicial complexes this simple starting triangulation looks good. Figure 5.23 shows the approximated Euclidean triangles for different initial simplicial complexes. Two of those have degenerated triangles from the beginning and the third has nearly degenerated triangles. These are images after the initialisation step, where each length should be approximately the same. Further

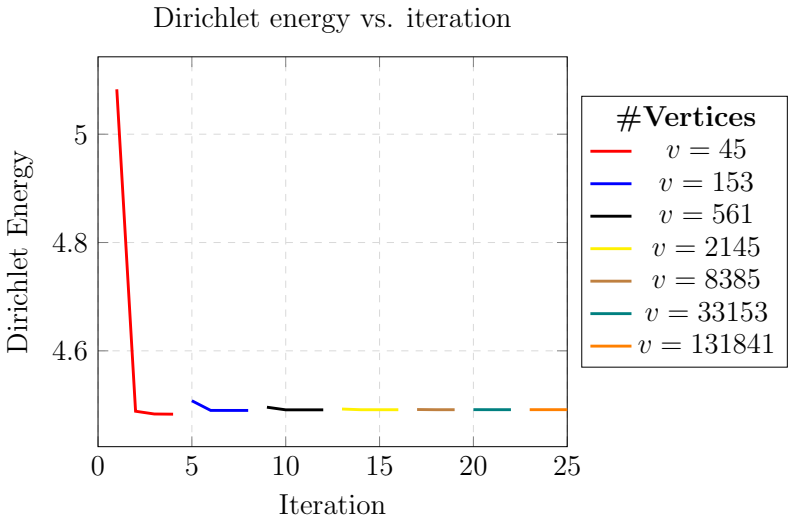

Figure 5.21: Convergence graph for close viscous rods.

refinements only increase the number of degenerated angles, hence this structure of the simplicial complex is not suited for this specific problem.

5.3 Summary

The previous examples show that with the help of the algorithm of Pinkall and Polthier and some modifications it is possible to compute discrete minimal surfaces in Riemannian manifolds and especially in shape spaces. In the Euclidean setting the algorithm performs quite well as expected. In the more complicated case and the first example of a Riemannian manifold, the Euclidean space $\mathbb{R}^3$ with a distorted metric as distance approximation, it can be seen that different initial simplicial complexes have an impact on the conformal structure of the triangulation and that an initialisation step to compute the initial data such that no angles are degenerated works and is even close to the optimum.
The last two examples showed that it is possible to compute discrete minimal surfaces in shape spaces. However, the convergence depends on a good triangulation depending on the specific setting. It is important to choose an initial simplicial complex suited for the initial shapes and computing initial interior vertices as starting-point for the optimisation step.

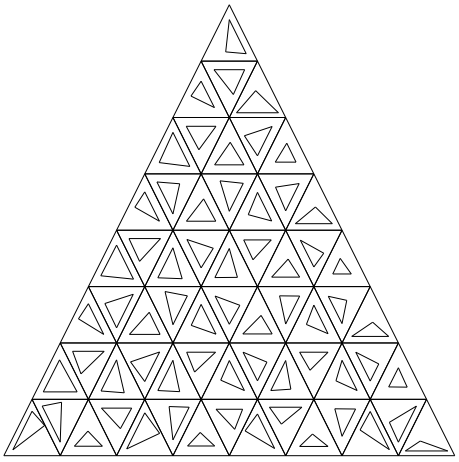

Figure 5.22: Approximated Euclidean triangles for the discrete surface of closed viscous rods.

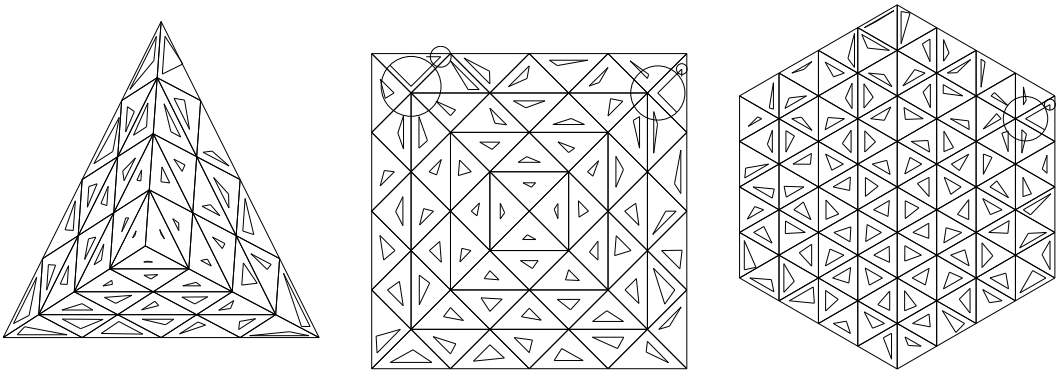

(a) t3 (b) t4 (c) t6

Figure 5.23: Discrete surfaces for the closed viscous rods with bad initial simplicial complexes. (a) has many triangles with angles $> \frac{\pi}{2}$ at the boundary, (b) and (c) have degenerated triangles. This shows the approximated Euclidean triangles after the additional initialisation step.

6 Outlook

While testing the algorithm a lot of triangles degenerated, either because one side was way too large, or because one side was way too small. This is a problem because if at one point during the algorithm a triangle is degenerated the algorithm diverges. This actually happened in a lot of case, however, by choosing carefully an initial simplicial complex and initialisation as presented in the closed viscous rods case, the algorithm converges. Pinkall and Polthier motivated in [PP93] further refinement steps when degenerations occurred during the process of the algorithm. A different way to avoid degenerated triangles is by computing better lengths and angles through the discrete geodesic calculus. However, the discrete geodesic calculus was only used in an initial step to compute the geodesics for the boundary curve. Computing all lengths and/or angles with this calculus is very expensive and early tests showed that the gain does not justify the computational efforts.
The reason why the Dirichlet energy converges to negative infinity in case of degenerated triangles in shape spaces is due to the distance approximations. These are neither symmetric nor do they satisfy the triangle inequalities. For a distance approximation which satisfies the triangle inequalities the Dirichlet energy is always positive. So better distance approximations could lead to fewer degenerated triangles.

Shape spaces can be interpreted as Riemannian manifolds. For a boundary curve disk-type minimal surfaces exist and the algorithm of Pinkall and Polthier can be applied to Riemannian manifold such that discrete minimal surface can be computed. These results motivate finding a proof for a convergence of the algorithm of Pinkall and Polthier in Riemannian manifolds. This seems, however, manageable in the case of finite-dimensional manifolds when the initial points are sufficiently close or by adding additional requirements to the injectivity radius and curvature such that the set of all possible discrete surfaces is compact again.

Pinkall and Polthier based their convergence theorem of the algorithm on the compactness of the set of possible surfaces. Here, the non-degeneracy condition implies compactness. Considering the set of all discrete surfaces with bounded Dirichlet energy which satisfy the boundary condition could lead to a similar compactness theorem in the finite-dimensional Euclidean case, allowing triangles to degenerate during the process. In both cases the existence of a discrete minimal surface which satisfies the boundary condition and has finite Dirichlet energy is needed anyway, so the set of all such discrete surfaces is not empty.

Furthermore,the algorithm of Pinkall and Polthier is not per-se limited to disk-type minimal surfaces. Given a different initial simplicial complex, the algorithm can compute discrete minimal surfaces for multiple boundary curves. This could work in Riemannian manifolds as well.

Considering the discrete geodesic calculus, this was only the next step, from discrete geodesics to two-dimensional minimal surfaces. It would be desirable to compute discrete minimal surfaces of higher codimension. That means that for example for k given objects in a shape space where for each $k-1$ subset of points there is a $(k-1)$-dimensional minimal surface connecting these $k-1$ points. The task is then to compute a discrete minimal surface of codimension k, bounded by these lower-dimensional minimal surfaces. In this case, however, even the theory does not provide the existence of smooth minimal surfaces, stronger requirements are necessary.

Moreover, only finite-dimensional Riemannian manifolds were treated, shape spaces in general are Hilbert manifolds and as such infinite-dimensional. Then the existence of continuous minimal surfaces is no consequence of the standard geometric measure theory and has to be further investigated.

List of Figures

Bibliography

[Alm93] F. J. Almgren. Questions and answers about area-minimizing surfaces and geometric measure theory, 1993.

[Cou37] R. Courant. Plateau's problem and dirichlet's principle. *Annals of Mathematics*, 38(3), 1937.

[Cou50] R. Courant. *Dirichlet's Principle, Conformal Mapping, and Minimial Surfaces*. Universitext. Springer-Verlag New York, 1950.

[DJK+10a] U. Dierkes, R. Jakob, A. Küster, S. Hildebrandt, F. Sauvigny, and A. Tromba. *Global Analysis of Minimal Surfaces*. Grundlehren der mathematischen Wissenschaften. Springer Berlin Heidelberg, 2010.

[DJK+10b] U. Dierkes, R. Jakob, A. Küster, S. Hildebrandt, F. Sauvigny, and A. Tromba. *Minimal Surfaces*. Grundlehren der mathematischen Wissenschaften. Springer Berlin Heidelberg, 2010.

[DJK+10c] U. Dierkes, R. Jakob, A. Küster, S. Hildebrandt, F. Sauvigny, and A. Tromba. *Regularity of Minimal Surfaces*. Grundlehren der mathematischen Wissenschaften. Springer Berlin Heidelberg, 2010.

[DL11] C. De Lellis. The regularity of minimal surfaces in higher codimension. *Memoirs of the American Mathematical Society*, 2011.

[DLS11] C. De Lellis and E. Spadaro. Almgren's q-valued functions revisited. *Memoirs of the American Mathematical Society*, 2011.

[Dou31] J. Douglas. Solution to the problem of plateau. *Trans. Amer. Math. Soc.*, 33, 1931.

[Fed69] H. Federer. *Geometric measure theory*. Grundlehren der mathematischen Wissenschaften. Springer, 1969.

[FF60] H. Federer and W. Fleming. Normal and integral currents. *Annals of Mathematics*, 72(3), 1960.

[FW06] T. Fletcher and R. Whitaker. Riemannian Metrics on the Space of Solid Shapes. In Xavier Pennec and Sarang Joshi, editors, *1st MICCAI Workshop on Mathematical Foundations of Computational Anatomy: Geometrical, Statistical and Registration Methods for Modeling Biological Shape Variability*, Copenhagen, Denmark, 2006.

[HKW76] S. Hildebrandt, H. Kaul, and K.-O. Widman. Dirichlet's boundary value problem for harmonic mappings of riemannian manifolds. *Mathematische Zeitschrift*, 147(3), 1976.

[HW07] F. Hélein and J. Wood. Harmonic maps, 2007.

[Jos08] J. Jost. *Riemannian Geometry and Geometric Analysis*. Universitext. Springer, 2008.

[KBCL09] D.G. Kendall, D. Barden, T.K. Carne, and H. Le. *Shape and Shape Theory*. Wiley Series in Probability and Statistics. Wiley, 2009.

[Ken89] D. G. Kendall. A survey of the statistical theory of shape. *Statist. Sci.*, 1989.

[Lan99] S. Lang. *Fundamentals of differential geometry*. Graduate texts in mathematics. Springer, New York, 1999.

[Mor48] C. B. Morrey. The problem of plateau on a riemannian manifold. *Ann. of Math.*, 49, 1948.

[Mor88] F. Morgan. *Geometric measure theory, a beginner's guide*. Academic Press, 1988.

[PP93] U. Pinkall and K. Polthier. Computing discrete minimal surfaces and their conjugates. *Experimental Mathematics*, 2(1), 1993.

[Rad30] T. Rado. On plateau's problem. *Annals of Mathematics*, 31(3), 1930.

[RW13] M. Rumpf and B. Wirth. Discrete geodesic calculus in shape space and applications in the space of viscous fluidic objects. *SIAM J. Imaging Sciences*, 6(4), 2013.

[RW15] M. Rumpf and B. Wirth. Variational time discretization of geodesic calculus. *IMA Journal of Numerical Analysis*, 35(3), 2015.

[Sim83] L. Simon. *Lectures on Geometric Measure Theory*. Lecture series. Australian National University, 1983.

[XDC88] S. Xu-Dong Chang. Two-dimensional area minimizing integral currents are classical minimal surfaces. *J. Amer. Math. Soc. 1*, 1988.